Dose Painting to Combat Tumor Hypoxia While Sparing Urethra in Prostate IMRT: A Biologically-Based Adaptive Approach Accounting for Setup Uncertainties and Organ Motion

by

Lingshu Yin

B.Sc. Nanjing University 2006

A THESIS SUBMITTED IN PARTIAL FULFILMENT OF THE REQUIREMENT FOR THE DEGREE OF

Master of Science

in

The Faculty of Graduate Studies

(Physics)

The University of British Columbia

(Vancouver)

October 2008

© Lingshu Yin

ABSTRACT

Enhanced resistance to radiation could be caused by both chronic hypoxia and acute hypoxic which has been reported in prostate cancer in various studies. Therefore currently used dose prescriptions (70Gy in 35 fractions) for external beam radiation therapy (EBRT) of prostate cancer has been suggested insufficient to provide optimum clinical outcome. In this study, we propose a Biologically Guided Radiation Therapy approach to boost dose in hypoxic prostate tumor regions while sparing the urethra. A previously proposed hypoxia model was modified for prostate cancer and incorporated into treatment plan optimization. The concept of equivalent uniform dose (EUD) was used in the optimization and evaluation of results. CT data from 25 prostate cancer patients who recently received EBRT at the British Columbia Cancer Agency (BCCA) and hypothetical hypoxic regions manually drawn on these CT scans were selected for this study. The results show that our methods could boost dose in target volume to substantially higher levels. EUD of planning target volume increased to more than 80Gy, despite accounting for effects of hypoxia. This increase was achieved with only minor changes in dose in normal tissues, typically less than 5Gy. Notably, urethra sparing was excellent with a EUD around 64Gy. Robustness of the proposed approach is verified against various hypoxic settings. EUD comparison between RT plans in biological guided and conventional approaches using the same RT technique (Volumetric Modulated Arc Therapy) also suggests that biologically guided radiation therapy (BGRT) approach is more suitable for dose painting purposes with the advantage of delivering sufficient dose to hypoxia region in different scenarios and sparing normal tissue better. Furthermore, we also investigated the impact of inter-fraction patient set-up error and intra-fraction organ motion on the high dose gradients achieved with this proposed dose painting method and explored the feasibility of adapting geometrical uncertainties (represented as systematic error and random error) into treatment planning. Image error obtained from EPID images are used to derive systematic uncertainty and random uncertainty. During the geometrical uncertainty adapted optimization, dose matrix in PTV is shifted based on systematic error and convolved with a Gaussian kernel which is pre-calculated using random error. CT sets and organ contours from five patients who enrolled in the previous dose painting

study are selected. For each of them, seven plans are generated using cumulated uncertainty data which was collected after every five fractions. We also present the outcome in terms of equivalent uniform dose (EUD). For four of the patients, EUD history of all seven plans suggests using the proposed optimization method with uncertainty data from the first five fractions, it is possible to achieve the same target coverage of static treatment plans (difference in EUD less than 1Gy). Meanwhile, the elimination of PTV margin also leads to a significant dose reduction (more than 15Gy) in rectum.

TABLE OF CONTENTS

LIST OF TABLES

LIST OF FIGURES

ACKNOWLEDGEMENT

First I would like to thank Dr. Vitali Moiseenko, my research supervisor who opened the door to Biologically Guided Radiation Therapy for me. His knowledge in both radiation therapy and radiation biology lit the wonderful world behind that door, his attitude to work and research always inspires me to explore it.

Dr. Karl Otto, my co-supervisor, gave me numerous help for treatment planning and programming. This two years' research work would be much tougher without his help and his humorous talks in my office.

Dr John North and Dr Mitchell Liu also provided tremendous help from a distinctive view as oncologists. The tedious contouring work and consultation with them are essentially the foundation of this work.

Last but not least, I would like to thank Mr Anthony Slowey for providing EPID data and walking me through it. I would be still puzzled by those EPID images and data without him.

CO-AUTHORSHIP STATEMENT

This project is an interdisciplinary work performed by the cooperation of graduate student (Lingshu Yin), medical physicists (Vitali Moiseenko, PhD and Karl Otto, PhD), and radiation oncologist (John North MD, and Mitchell Liu, MD). Chapter 2 of this thesis is coauthored with Vitali Moiseenko, Karl Otto, John North and Mitchell Liu. Chapter 3 of this thesis is coauthored with Vitali Moiseenko, Karl Otto and Mitchell Liu.

Lingshu Yin, the first author of each chapter, is the primary researcher in this work. He did the treatment planning, Matlab programming, data collection, data analysis, paper writing, and public presentation.

Dr. Vitali Moiseenko, medical physicist in BCCA-Vancouver Cancer Centre, is the research supervisor of Lingshu Yin. He proved the general idea of this work. During the research, he was closely involved, giving instructions and guiding the direction of this work.

Dr. Karl Otto, medical physicist in BCCA-Vancouver Cancer Centre, is the co-supervisor of Lingshu Yin. He provided prototype code of Volumetric Modulated Arc Therapy as a treatment planning platform, and gave suggestions on this work.

Dr John North, radiation oncologists from Dunedin Hospital New Zealand and Dr. Mitchell Liu, radiation oncologist in BCCA-Fraser Valley Centre, proved the patient data and gave suggestions from oncologists' point of view.

CHAPTER 1. Introduction

Approximately 1 in 3 Canadians will be diagnosed with cancer in their lifetime. The goal of radiation therapy is killing tumor cells or shrinking tumor before surgery or chemotherapy to achieve complication free survival. Based on the statistics from the British Columbia Cancer Registry, approximately 20,000 new patients were diagnosed with cancer in the year 2005 with more than 150,000 visits to the four cancer centers in BC Cancer Agency for radiation therapy. Radiation therapy (RT) is an important part of cancer treatment, it works by causing breaks in cellular DNA leading to irrepairable damage and cancer cell death. RT was first used over 100 years ago, since then delivery techniques have become much more sophisticated allowing increased radiation doses to be delivered to a more conformal target volume while minimizing dose to the normal surrounding tissues. As a result the survival and local control rates of many cancers has risen dramatically. However, there is a continuing need to improve radiation delivery techniques and in particular to spare the normal tissue toxicity which leads to much of the morbidity of RT treatment.

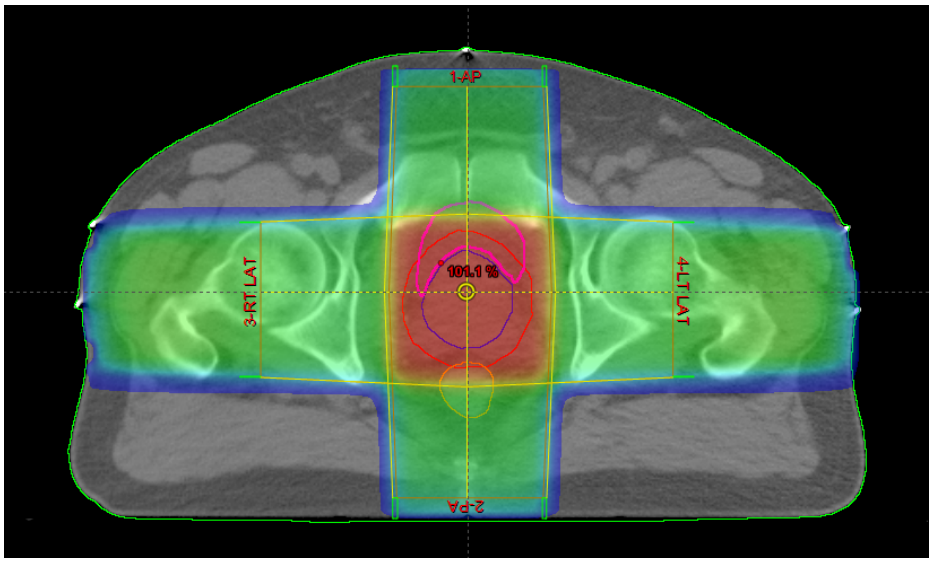

Figure 1.1: A sample radiation therapy plan for patients with prostate cancer. Four radiation beams come from anterior, posterior, left lateral and right lateral directions to deliver curative dose to tumor in the center meanwhile sparing the normal tissue including bladder, rectum and femoral heads.

A complete course of radiation therapy (RT) requires the co-operation between radiation oncologists, medical physicists, radiation therapists and dosimetrists. Radiation oncologists are specialist physicians with a particular expertise in treating cancer with radiation. A radiation oncologist is responsible for overall decisions regarding radiation treatment of a particular patient. These decisions are made in consultation and with informed consent of a patient. In particular, treatment modality (external beam radiation therapy or brachytherapy), prescribed dose, dose per fraction are decided by a radiation oncologist. Furthermore, target volumes are delineated, or contours drawn by dosimetrists, are approved and dose constraints are decided for both target volumes and organs at risk. Radiation oncologists monitor the patient's progress through the treatment and follow-up the patient after radiation therapy is finished. Dosimetrists are responsible for producing a radiation therapy plan which complies with objectives set by a radiation oncologist. In case of advanced treatment techniques, for example intensity-modulated radiation therapy (see described in more detail below), this requires in-depth understanding of aspects of RT including patient set-up, immobilization, optimum field arrangement and choice of beam energy. The role of the medical physicist is to ensure the quality of radiation therapy. This involves commissioning of the treatment planning systems (TPS), calibration and quality assurance of linear accelerators and plan checking. Therapists are responsible for actual dose delivery. The knowledge of radiation therapy

encompasses breadth of disciplines, specifically radiation physics/chemistry, radiation biology, radiation oncology and medical physics. In this chapter, we will start from introducing radiation physics and chemistry, explaining the process of energy deposition in tissue at a fundamental level. This will be followed by a description of aspects of radiobiology relevant to evolution of cell damage from primary energy deposition to lethal lesions. Means to modify cell kill using dose rate or microenvironment will be introduced and formalism to quantitatively describe cell survival as a function of dose, while accounting for modifying factors, will be presented. The effects of radiation on tumor and normal tissue and the advances in medical physics to improve the quality of radiation therapy are discussed at the end of this chapter.

1.1. Background in Radiation Physics and Radiation Biology

1.1.1. Physics and Chemistry of Radiation Absorption

Therapeutic X- and γ-rays mainly consist of high energy photons which will not directly change the molecular structure or bring chemical and biological damage to cells. However when photons are absorbed in the material, their energy is passed to fast-moving electrons which leads to direct energy depositions in the sensitive target inside a cell, which is now firmly established as DNA, and also production of radicals following ionizations and excitation in water molecules. The latter leads to a series of chemical reactions which produce DNA lesions. These two pathways of DNA damage are called direct and indirect effects. While most of the DNA damage is successfully repaired, mis-repair and incomplete repair lead to formation of lesions which may ultimately cause cell death or transformation.

In general, radiation can be classified as ionizing radiation and non-ionizing radiation. If the charged particle (electrons) in an atom or molecule can be raised to a higher energy lever by radiation without ejection of electrons, the radiation can be called non-ionizing radiation. In contrast, ionizing radiation is the radiation which can cause ejections of electrons in the atom or molecules and it is the radiation most used in radiation therapy. Based on the energy of photons (500keV~12MeV commonly used in clinic), three kinds of interactions (photoelectric absorption, Compton scattering and pair production) dominate the entire process.

Eighty percent of cells are composed of water, thus we can use water to study how radiation is absorbed. Water molecules can be ionized by photons or electrons, which is a predominant path of energy deposition in photon irradiation.

$$H_2O \rightarrow H_2O^+ + e^- \quad (1.1)$$

Ionized water molecule lose a free electron, thus has an un-paired electron and an extremely short life, on the order of 10^{-10} second [1]. The ionized water molecule reacts with another water molecule by donating a proton, thereby leading to a production of a hydroxyl radical which is highly reactive and may change the chemical bonds of other molecules.

$$H_2O^+ + H_2O \rightarrow H_3O^+ + OH\bullet \quad (1.2)$$

Radiation damage relevant to cell kill principally comes from the damage to DNA, which is directly or indirectly brought by photons, electrons and free radicals like hydroxyl radicals mentioned above.

1.2. Course of Cell Death

1.2.1. DNA Strand Breaks and Chromosomal Aberrations

The double helix structure of deoxyribonucleic acid (DNA) is widely acknowledged. DNA double helix consists of a sugar-phosphate backbone and bases which are connected by hydrogen bonds. Each base has a complementary base on the opposite strand. Radiation-induced biological effect relevant to cell lethality starts from DNA breaks produced by charged particles and the other chemical species, hydroxyl radicals being the most important of the species. Single or both strands can be damaged by radiation at the same time (Figure 1.2), however only double-strand breaks (DSB) are considered to be the most important ones which lead to chromosome aberrations, some of which are lethal [1].

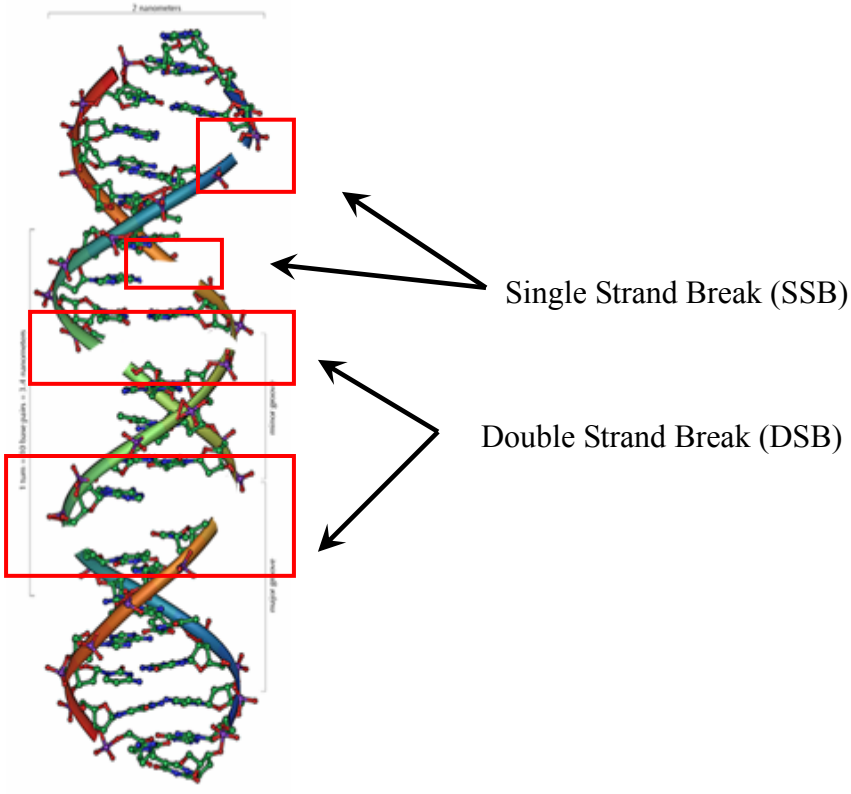

Figure 1.2: Illustration of single strand break and double strand break in DNA double helix structure.

Single-strand break (SSB), as its name suggests, is the break in a single strand. Because of the complementary base on the other strand, it is relatively easy to repair and preserve genetic information in DNA intact, thus DNA integrity is maintained. Double-strand break (DSB) are close single-strand breaks on both strands (distance smaller than 10 base pairs) [2][3]. DNA integrity is no longer maintained thus it is more difficult to repair a DSB correctly.

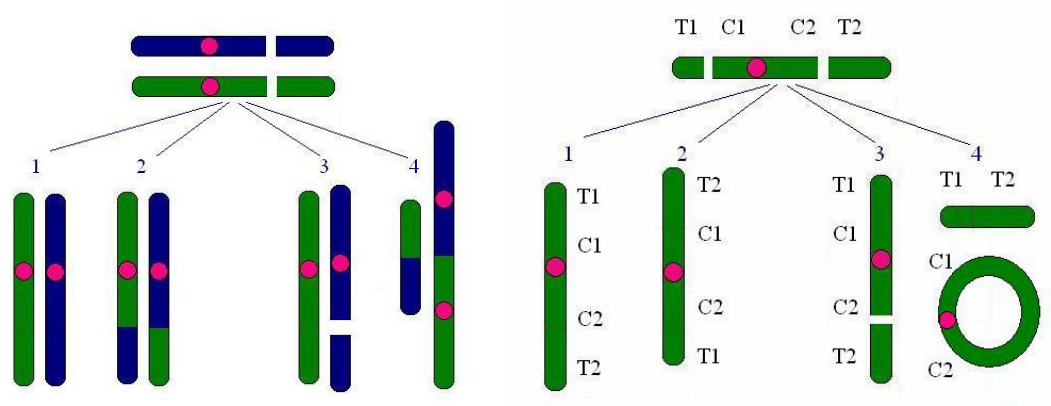

1. Full repair
2. Symmetric translocation
3. Incomplete repair
4. Dicentric

1. Full repair
2. Inversion
3. Incomplete repair
4. Centric ring

Figure 1.3: Possible outcomes for two radiation-induced double-strand breaks in two (left panel) or one (right panel) chromosomes. Outcomes 1 are faithful restitution, 2 are exchanges (translocations) which would not interfere with cell division, 3 and 4 are incomplete repair and exchange which would interfere with cell division. (Courtesy Dr. Vitali Moiseenko)

DNA strand breaks can be produced by direct energy depositions in DNA, which may cause either direct dissociation or loss of hydrogen from one of the carbon positions in

the sugar ring. In the latter case a sequence of events leading to elimination of a phosphate group occurs. In the case of indirect action, hydroxyl radicals are the most important species as far as DNA breaks are concerned. There is a consensus that a hydroxyl radical abstracts a hydrogen from a carbon position in the sugar ring. This is followed by a phosphate elimination from either C_3' or C_5' position and consequently a SSB. While other reactive species are capable of interacting with DNA, their reaction rates are either too low, or their reactions are restricted to those with bases, which means that sugar-phosphate backbone remains unaffected. For example, hydrated electrons, e^-_{eq} react with bases by adding to double-bonds or abstracting hydrogen atoms from carbon positions. Following reactions between reactive species and DNA bases, chemical decay of bases will also lead to DNA lesions. However, mutation rates in mammalian cells are quite low which suggests the underlying complex repair mechanisms of DNA. Various pathways have been suggested as effective method to repair single-strand break or double-strand breaks, such as base excision repair, nucleotide excision repair, non-homologous end joining, etc. A moderate dose can significantly increase the rate of DNA lesion to a level where the damage can not be totally fixed. There are 40-60 DSB produced per Gy in a mammalian cell, and typically 2-3 Gy of X- or γ-rays reduce cell survival to 37% (1/e expressed in percent). Fatal mis-repaired or un-repaired DNA damage (Figure 1.3) result in chromosome aberrations interfering with cell division (lethal lesions) and therefore cell death. This means that divisions cannot be sustained. In contrast, non-fatal chromosome aberrations will result in transformed cells, i.e., while a cell is capable of sustaining divisions, its genetic code is corrupt. Most cells containing lethal lesions will not die immediately after being irradiated. During or after its cell

division, fatal chromosome aberration result in the failure to complete mitosis. This is why this pathway of cell inactivation is called mitotic or reproductive death. Interphase death, when a cell is not able to reach mitosis, while playing minor role for external beam therapy, can be pronounced in special circumstances, for example under low dose rate conditions.

1.3. Dose Response of Normal Tissue and Tumor

1.3.1. Repair, Reassortment, Repopulation and Reoxygenation

In conventional multifraction radiation therapy, the effect of fractionation has been summarized as repair of sublethal damage, reassortment of cells within the cell cycle, repopulation and reoxygenation, well known in radiation biology as “4Rs”.

Repair of sublethal damage (double-strand breaks), involves various chemical pathways which replace modified chemical compounds to their original state.

A complete cell mitotic cycle consists of four distinct phases, mitosis phase (M), DNA synthetic phase (S) and two gaps (G1, G2) between M and S phase. Generally cell in its late S phase are more resistant to radiation than cells in other phases, whereas cell in G2/M phase is most sensitive [4] (**Figure 1.4**).

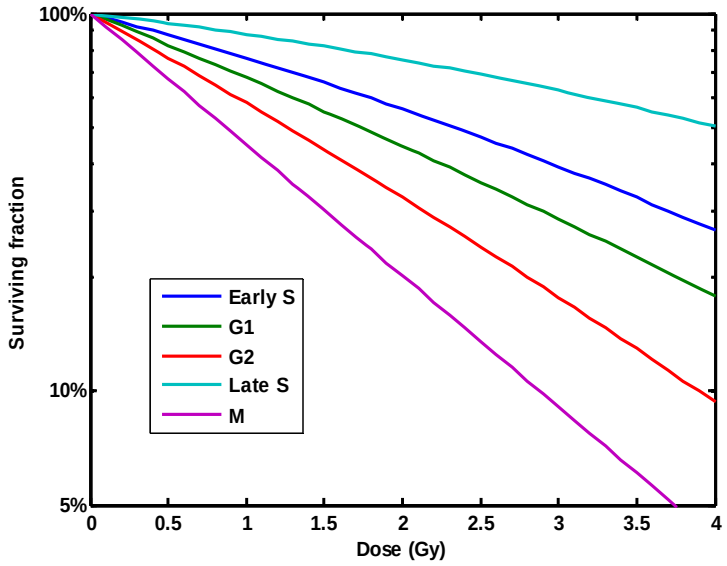

Figure 1.4 Phase specific survival curves calculated for Chinese hamster lung cells (V79)

If an asynchronous population of cells is exposed to radiation, more cells in sensitive phases are killed, thus the entire population tends to be synchronized and resistant to radiation. This phenomenon suggests that fractionated radiation therapy would benefit from cell population "reassortment" among stages of cell cycle during the time interval between fractions. Thereby, in fractionated dose delivery proliferating cells will unavoidably get irradiated in a sensitive stage of the cell cycle.

Repopulation, as its name suggests, is the reproduction of cells which leads to increased surviving fraction. Reoxygenation refers to the oxygen effect on hypoxic cells which is more resistant to radiation than oxygenated cells. It will be discussed in detail in Chapter 2.

1.3.2. Cell Survival Curves

Since the first *in vitro* survival curve for *mammalian* cells irradiated with x-rays was

reported by Puck et al in 1956 [5], various models have been proposed to fit cell survival curves, among them the linear quadric (LQ) model is the most widely accepted one:

$$SF = e^{-(\alpha D+\beta D^2)}, (1.3)$$

where *SF* is surviving fraction, *D* is dose delivered in acute fashion, α and β are the model parameters. Acute in this context means that time to deliver the dose is too short for repair to take place.

Assuming that the number of lethal lesions is distributed among cells according to the Poisson distribution, if a single cell is exposed to a single acute dose *in vitro*, the probability of this cell containing zero lethal lesions is:

$$P_0 = e^{-\bar{L}}, (1.4)$$

where P_0 is the surviving probability, $\bar{L}$ is the averaged number of lethal lesions per cell. Therefore, by comparing Eq 1.3 and 1.4, $\alpha D + \beta D^2$ can be interpreted as the average number of lethal lesions per cell. The α terms relates to lethal lesions caused by one electron track (yield proportional to Dose), whereas β term relates to lethal lesions produced following binary exchanges of sublethal lesions caused by two electron tracks (yield proportional to Dose^2). Because the quadratic term requires the presence of two DSB in the same cell at the same time, it is dose-rate-dependent. In the limit, when dose rate is very low, by the time the second DSB is produced by a particle track traversing the cell, the first DSB would get repaired. Therefore, in this limit the quadratic component would disappear. In case of multi-fraction dose delivery, with each fraction acting independently, i.e., time between fractions is sufficient to allow for full repair, the probability to survive all fractions is the product of probabilities to survive each fraction.

In case of equal dose per fraction and each fraction delivered in an acute fashion, the linear quadric model can be modified to take account of dose fractionation

$$SF = e^{-(\alpha d+\beta d^2)N} = e^{-(\alpha Nd+\beta Nd^2)} = e^{-(\alpha D+\beta dD)} \text{ , (1.5)}$$

where D is total dose delivered in N fractions and d is the dose per fraction.

1.3.3. Dose Rate Effect and Biological Effective Dose (BED)

Dose fractionation is widely used in radiation therapy. From the LQ formalism described above, it is clear that cell survival, and consequently RT outcome, will depend on both dose and dose per fraction (or dose rate in the case of brachytherapy). For example, if a total dose of 70Gy is prescribed to be delivered to prostate, this dose alone is insufficient to project the RT outcome. The treatment in 35 fractions (2Gy/fraction) or 30 fractions (2.33Gy/fraction) will have different outcomes. To account for dose per fraction effect and compare alternative fractionation schedules a surrogate dose index which takes dose per fraction or dose rate effect into account is required.

Eq 1.5 can be used to derive the concept of biological effective dose (BED),

$$BED = D \times (1 + \frac{d}{\alpha / \beta}) \text{ , (1.6)}$$

which inherently includes the biological effect of different dose fractionation schedules. Survival fraction is connected to BED through:

$$SF = e^{-\alpha \times BED} \text{ (1.7)}$$

To calculate the BED value from a given dose delivery schedule, the only parameter required is α/β. Values of this parameter are available from *in vitro* experiments and can be derived for both normal tissues and tumor response from clinical follow up of cancer patients treated with radiation therapy. This value is important in fractionated dose

delivery as it illustrates the relative response of tumor and normal tissues under different dose rate/dose fractionations. It is also indispensable in order to choose a appropriate dose schedule for particular cancer.

The value of α/β for late responding normal tissues is relative small which shows the importance of dose per fraction, *d*, whereas α/β for tumor is larger which shows the importance of total dose *D* (Table 1.1).

Table 1.1 Selected α/β values for tumor and normal tissue

Organ	α/β (Gy)	Reference:
Skin cancer cells	8.4	Thames et al 1990[6]
Well oxygenated human prostate cell lines	8.3	Nahum et al 2003 [7] Orton 2004 [8]
Prostate cancer cells	1.5	Brenner and Hall 1999[9]
Bone (stricture/perforation)	2.2 - <8	Thames et al 1989[10]
Lung (pneumonitis)	<3.8	Thames et al 1989[10]
Oropharynx	4.5	Thames et al 1989[10]

Generally, late response in normal tissue is more sensitive to dose delivered per fraction during radiation therapy, whereas tumor response is more sensitive to total dose. This is the direct evidence supporting the current dose schedule setups in external beam radiation therapy (usually ~2Gy/fraction).

While α/β for most tumors was shown to be high, in specific cases it might be as low as that for normal tissue. It has been reported that prostate cancer may not response to radiation as other tumors. α/β reported by Bernner and Hall (0.8~2.2Gy) [9] is significantly smaller than other tumors (typically ~10Gy). If α/β is truly as low as reported, increasing amount of dose per fraction, i.e. hypo-fraction, will result in better tumor control. Based on the available proof of low α/β for prostate cancer a number of hypo-fractionated RT clinical trials have been carried out or are in progress. If outcomes

match expectations, this would validate this low α/β ratio. A simple calculation of *BED* using different dose schedules can well illustrates the reason of hypo-fractionation for tumors with low α/β values. As shown in Table 1.2, increasing dose per fraction from 2Gy to 2.94Gy can boost tumor BED from 84Gy to 174.05Gy with only minor change in BED of normal tissue. If this change in BED agrees with the clinical outcome from current hypo-fraction trials, there would be strong evidence supporting that the α/β value of prostate tumor is much lower than the nominal value (10Gy).

Table 1.2: Comparison of BED in conventional and hypo-fraction schedule.

		α/β (Gy)	Dose per fraction (Gy)	Number of fractions	Total Dose(Gy)	BED (Gy)
Conventional schedule	Tumor	10	2	35	70	84
	Normal tissue	3	2	35	70	116.67
Hypo-fraction schedule	Tumor	1.5	2.94	20	58.8	174.05
	Normal tissue	3	2.94	20	58.8	116.42

1.3.4. Volumetric Response

Response to radiation on a cellular level has been well explored, whereas the response of normal tissue as a structure is more complicated. This is because while for tumors an assumption that inactivation of a particular cell has little effect on response of adjacent cells, for organs at risk, tissue and organ levels of organization cannot be ignored. Normal tissue can be divided into numerous functional sub-units (FSU). Depending on the organization of FSUs, normal tissue falls on a spectrum between two extremely idealized cases: serial organ and parallel organ. As terminology indicates, similarities to electric circuits apply. This is further illustrated in the Figure 1.5 using an example of Christmas

lights, incapacitation of an organ would exhibit as the tree on the right side not lit. As it is shown in Figure 1.5, in serial structures, one incapacitated FSU will cause failure of the entire organ (upper panel). In parallel structures, it might still work after one or several FSU are incapacitated by radiation (lower panel).

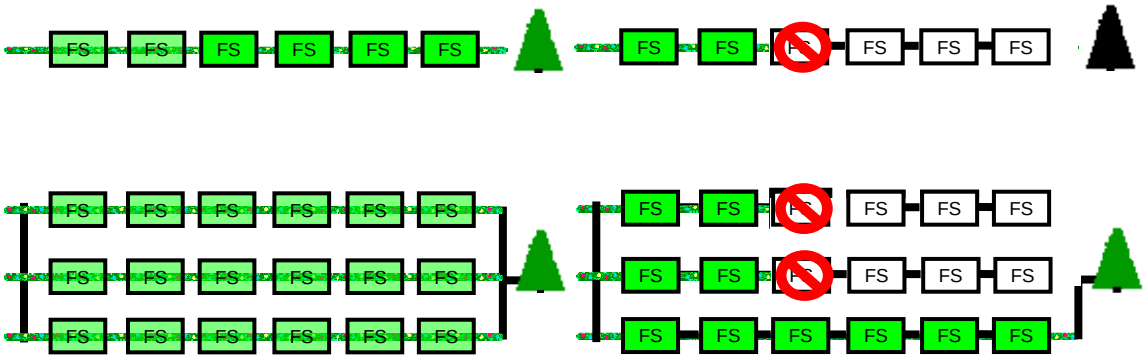

Figure 1.5: Mechanisms of volumetric response in serial organ and parallel organ.

(Courtesy Dr. Mitchell Liu)

Examples shown above offer a very simplified illustration, however it well explains the reason why serial structures are very sensitive to hot spots in dose distributions whereas parallel structures are more sensitive to the average dose of the entire volume. One hot spot in a serial structure can destroy one FSU and thereby incapacitate the whole organ. In contrast, in organs with parallel organization, compensatory mechanisms exist. While normal tissue will be destroyed in the region of the hot spot, the remaining FSU will compensate for the loss of function.

Dose Volume Histograms (DVH) are routinely used in the clinic to set planning objectives and to evaluate treatment plans. For example, dose-volume constraints intended to minimize normal tissue toxicity were suggested in RTOG 0126 for prostate cancer patients treated with external beam radiation therapy [11]. For rectum, no more than 15% volume can receive a dose exceeding 75Gy; no more than 25% volume can

receive a dose exceeding 70Gy; no more than 35% volume can receive a dose exceeding 65Gy; and no more than 50% volume can receive a dose exceeding 60Gy. This means that a DVH curve for rectum should not exceed those constraint points indicated by red arrows in Figure 1.6.

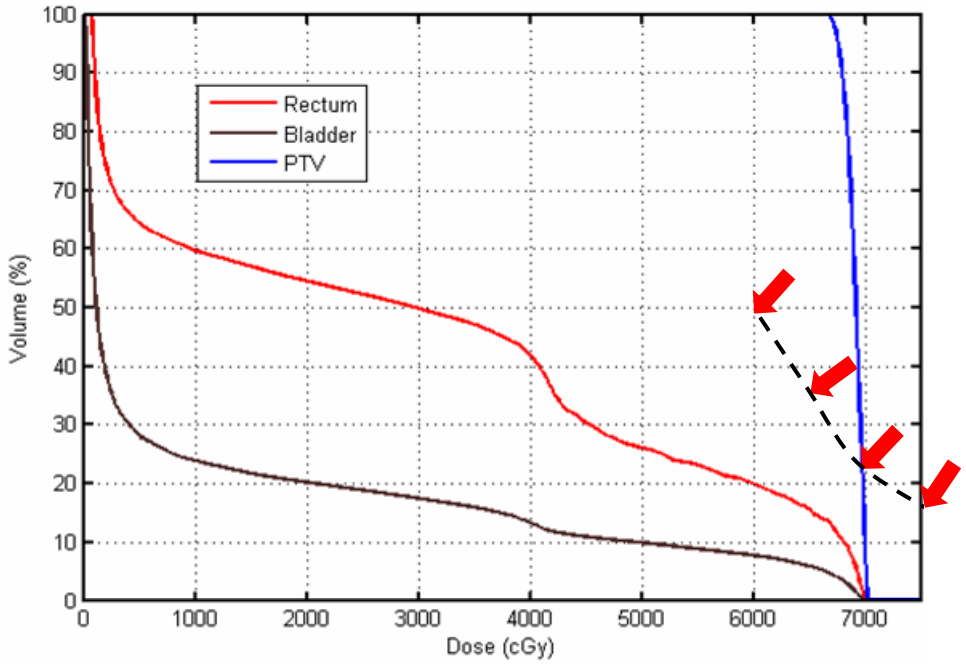

Figure 1.6: A sample Dose volume histogram. Dose-volume constraints for rectum are suggested in RTOG 0126 [11].

In addition to evaluating a plan, the DVH can be used to choose the best plan from a set of competing plans produced by a dosimetrist. However, an often encountered problem in treatment planning is that the DVH curves from two competing plans cross. As shown in Figure 1.7, rectum DVH curves in both plans comply with RTOG 0126 dose-volume constraints. However, the blue curve indicates that a small portion of rectum would receive a higher dose in this plan whereas in the other plan (red curve) a much larger portion of rectum would receive a smaller dose. Plan ranking in this case is not trivial because the importance of a small hot (large dose) region has to be compared to

that of a large region receiving moderate dose.

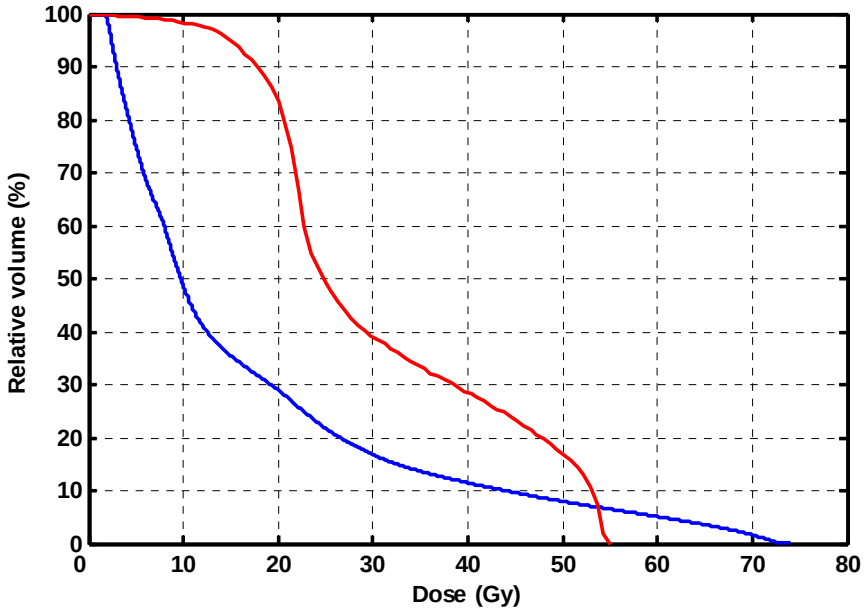

Figure 1.7: Illustration of crossing DVH curves

To address this issue, the concept of effective dose was proposed based on partial volume data [12] in order to describe the effect of inhomogeneous dose on tissue and its volume effect:

$$D_{eff} = \left(\frac{1}{N} \sum_{i=1}^{N} D_i^{1/n} \right)^n \quad (1.8)$$

D_{eff} is the uniform dose which will have same biological effect on tissue as the inhomogeneous dose distribution. D_i is dose to voxel and N is the number of voxels. n is the parameter which describes volume response of an organ Table 1.3. D_{eff} is close to maximum dose in the DVH if n is small, whereas it will be mean dose if n equals to 1.

Table 1.3 n parameters reported in literature [13]

Organ	n
Lung	0.87
Bladder	0.5
Brain	0.25

Femoral head and neck	0.25
Rectum	0.12
Esophagus	0.06
Spinal cord	0.05

As it is shown in the table, response of a parallel organ, such as lung, is sensitive to mean dose. Serial organs, such as, spinal cord and esophagus, with a smaller *n* are more sensitive to maximum dose. D_{eff} is designed to give the uniform dose distribution which is isoeffective to the inhomogeneous dose distribution from which it was derived. D_{eff} values calculated from DVHs shown in Figure 1.7 indicate that the plan shown as a red line (D_{eff} =42.33Gy) will provide better rectum sparing than the plan shown as a blue line (D_{eff} =56.5Gy). This means that hot spots outweigh large regions receiving moderate doses in term of treatment-related complications in this particular treatment plan.

1.4. Conformal Radiation Therapy

1.4.1. Volume Definitions

In clinical practice, eradication of the primary tumor while sparing surrounding normal tissue is the major objective of radiation therapy. A set of target volumes was defined by the International Commission on Radiation Units and measurements (ICRU), each target volume designed to account for specific features of tumor biology and geometric uncertainties associated with fractionated irradiation. As defined in ICRU Report 50[11], gross tumor volume (GTV) is "*the gross palpable or visible/demonstrable extent and locations of malignant growth*"; clinical target volume (CTV) is "*a tissue volume that contains a demonstrable GTV and/or subclinical microscopic malignant disease, which has to be eliminated*". "*This volume thus has to be treated adequately in order to achieve the aim of therapy, cure or palliation*". The goal of radiation therapy is to ensure that the

CTV receives a curative dose prescribed by the radiation oncologists. However, several factors hinder this goal. The setup error of patients' position before each treatment, intra- and inter-fraction organ motion and deformation during the treatment, leads to geometrical misses and therefore a different dose distribution in CTV compared to that originally planned. Thus a geometrical volume concept: Planning Target Volume was suggested in ICRU Report 50[11]: "*The Planning Target Volume (PTV) is a geometrical concept, and it is defined to select appropriate beam sizes and beam arrangements, taking into consideration the net effect of all the possible geometrical variations and inaccuracies in order to ensure that prescribed dose is actually absorbed in the CTV*". In practice, PTV is usually contoured as CTV plus a safety margin with the size of margin dependent on tumor site and clinical protocol used. Specifically, for lung cancer patients, organ motion due to breathing is substantial, therefore margins have to be large. However, if advanced methods, such as gating or tracking are used, the margins can be reduced.

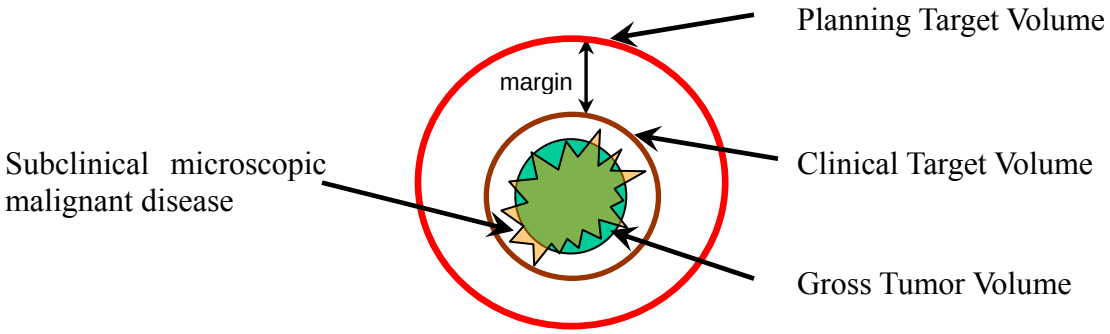

Figure 1.8: Volume definitions used in radiation therapy as defined in ICRU Report 50 [11]

The optimization of a radiation therapy treatment plan is usually done using a "forward" planning or "inverse" planning. In forward planning, the decision of beam

orientation, collimator setup and other parameters are made manually, and it is usually used in conformal radiation therapy. However, in intensity modulated radiation therapy (IMRT), due to the complexity of treatment planning, it is conducted as inverse planning. Dose coverage of PTV and normal tissue sparing, can be translated into a simple numeric value, f i.e., treatment plan is designed in a trial and error iteration process in which treatment parameters are automatically adjusted based on the outcome from current setup and predicted setup until the outcome reaches a global minimum or maximum. Thus from the mathematical perspective, the process of treatment planning is therefore simplified to an optimization problem:

$$\max f(x) \text{ or } \min f(x);\ f \in R, x \in R^n \quad (1.9)$$

The purpose of the optimization is to adjust at least one of the following: beam orientation, intensity map and collimator setup. This is performed manually or automatically to minimize or maximize this value *f*, thus generating the treatment plan which satisfies the goal of radiation therapy.

The function *f* used to evaluate the dose distribution in target volumes and normal tissues is called an objective function or cost function. The most commonly used one is least square function:

$$f = \sum_{i,j} w_j \left(D_{ij} - D_j^p\right)^2 , \quad (1.10)$$

where w_j is the weight of structure j which renders the relative importance of each structure in radiation therapy. D_{ij} is the dose in ith voxel in structure j, D_j^p is the prescription or desired dose in structure j. The treatment planning program will search the solution space to find a plan which minimizes f thus reducing the difference between delivered dose D_{ij} and prescribed or desired dose D_j^p. This equation is an over-simplified

one as it is impossible to give each structure a uniform dose and it ignores the dose volume constraints required by radiation oncologists. To comply with dose-volume constraints and minimum/maximum dose constraints for both targets and organ at risk (OAR), a more sophisticated objective function is usually used [14].

$$f = \sum_i f_i^{\text{target}} + f_i^{\text{OAR}},$$

$$f^{\text{target}} = \frac{1}{N}\left(w_{low} \cdot \sum_j H(D_{low} - D_j) \cdot (D_j - D_{low})^2 + w_{high} \cdot \sum_j H(D_j - D_{high}) \cdot (D_j - D_{high})^2 \right),$$

$$f^{\text{OAR}} = \frac{1}{N}\left(w \cdot \sum_j H(D_j^{V_{x\%}} - D_{Vx}) \cdot (D_j^{V_{x\%}} - D_{Vx})^2 + ... \right),$$

, (1.11)

w_{low} and w_{high} are weights for maximum and minimum dose (D_{low} and D_{high}) constraints in target. D_j is dose in jth voxel, N is total number of voxels in ith structure. w is the weight for each dose-volume constraints in the OAR. $V_{x\%}$ is the $x\%$ "hottest" volume of a OAR, D_{Vx} is the dose constraint for this sub-volume. For example, no more than 25% of rectum volume can receive dose exceeding 70Gy in RT, this will set $D_{V25\%}$ equal to 70Gy. If dose of any voxel in this sub-volume $V_{25\%}$ notated as $D_j^{V_{x\%}}$ exceeds 70Gy, the objective function will be punished by the Heaviside step function (Eq.1.12):

$$H(D_1 - D_2) = \begin{cases} 1, D_1 > D_2 \\ 0, D_1 < D_2 \end{cases}, \quad (1.12)$$

This step function is also used in the objective function of targets to allow for minimum and maximum dose constraints in targets thus achieving PTV dose homogeneity (Eq.1.11).

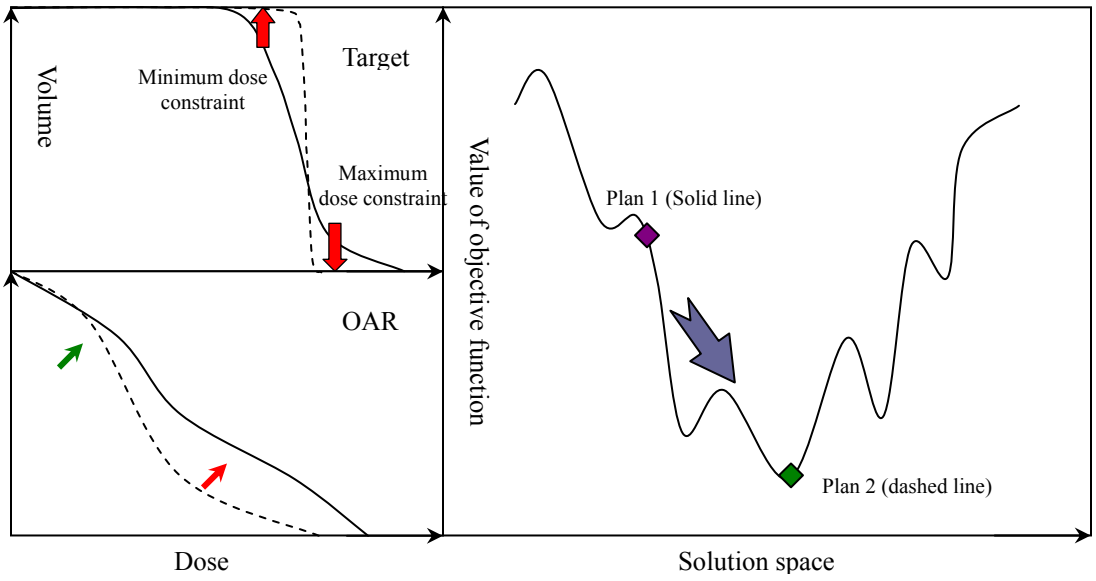

Figure 1.9 Sample of minimum/maximum dose constraints for target volume (top left panel) and dose-volume constraints for OAR (bottom left panel). Plan 2 (dashed line) is considered superior to Plan 1(solid line) as judged from objective function (right panel).

Figure 1.9 above shows how this objective function works. Plan1 (solid line) doesn't meet the minimum and maximum dose constraints for target (red arrows in upper left panel) whereas plan2 (dashed line) does. For OAR, plan1 meets the first dose volume constraints (green arrow in lower left panel), but it doesn't meet the second one (red arrow). Plan 2 meets both. Using the Heaviside step function, the cost value of plan1 is higher than plan2. The optimization engine embedded in the treatment planning software will iteratively adjust plan 1 to minimize this cost value, thus achieving its global minimum which is represented by plan 2 in the solution space.

1.4.2. Biologically Guided Radiation Therapy (BGRT) Examples

A thorough evaluation of a treatment plan should include the ultimate biological outcome

of the plan, prognosis for tumor control, likelihood and severity of complications after radiation therapy, quality of life, probability of secondary cancers, etc. Although it is difficult to predict individual response prior to radiation therapy, population based response data are widely available in radiation oncology and it is feasible to incorporate these data into treatment planning. However as seen from above, during the optimization process, the evaluation of a treatment plan is performed by the planning program based on an objective function which only uses dose as an outcome substitute. The connection from dose to biological outcome is ignored in the planning process. The dose volume constraints used in planning are based on clinical studies which define the biological meaning of least-square like objective functions, however with advanced medical imaging techniques (PET, SPECT, MRSI, etc) several inadequacies of these least square like objective functions have been reported.

First of all, in conventional practice, it is assumed that tumor cell density and radio-sensitivity are uniform, thus dose homogeneity in PTV is required. In RTOG 0126[11], it is required that dose inhomogeneity in PTV should be no larger than 7% (maximum dose to 2% of PTV or less should be under 107% of prescription dose). Hot spots in excess of 110% are regarded as major variations. However, various studies have reported that tumor cell density and radio-sensitivity are not uniform in the tumor volume. Dose boosting and dose painting are currently used in order to give extra dose to high risk regions.

Secondly, geometrical information is ignored when formulating the DVH from the dose distribution. Functional images acquired with single photon emission computed tomography (SPECT) from lung cancer patients demonstrated that normal lung has

inhomogeneous perfusion ability (Figure 1.10). Using BGRT with the guidance from SPECT, it is feasible to generate treatment plans with the same DVH but better dose function histogram (DFH) as compared to conventional RT plans [15]. Thus by appropriate sparing of high perfusion regions in normal lung, we can reduce the probability of having post radiation pneumonitis or fibrosis.

Figure 1.10: A fused SPECT/CT scan of a patient with lung cancer. The clear difference of patient's right lung as defined by SPECT and CT provides opportunity of sparing well functioning lung during radiation therapy.

The unique feature of BGRT is that the objective function used in treatment plan optimization can be highly patient or tumor type specific. For example, in radiation therapy for lung cancer, the relationship between dose and post-radiation perfusion is available [16][17], thus a specific objective function for lung cancer can be formulated to give the total probability of having post-radiation therapy pneumonitis. Using this objective function, the goal of treatment planning is to minimize the probability of

complication which inherently includes presently used dose volume constrains. In conventional RT, least square like functions are used regardless of tumor type, discrepancy between population based dose volume constraints and patient specific response is ignored. Combing dose matrix with functional information matrix, e.g. perfusion SPECT scan, into the objective function also overcomes the limitations of dose volume constraints: the lack of spatial information.

Numerous models have been proposed for BGRT [18]. These models can be based on either empirical models or theoretical mechanistic models. Both can be incorporated in objective functions and treatment planning. An empirical or phenomenological model is a model which describes observations by fitting data without assumptions to underlying mechanisms governing the response. Mechanistic models start by describing underlying processes in radiation effect. Development connects them to experimental or clinical data. Currently the boundary between empirical and mechanistic models is not very clear, as most mechanistic models will contain adjustable parameters to fit experimental data. While these parameters do have a mechanistic meaning, because their values often cannot be independently validated the mechanistic nature of the model is eroded.

One main trend in BGRT research is using biologically-weighted dose such as equivalent uniform dose (EUD) or effective dose as indices for optimization. This approach accounts for the biological effect when interpreting an inhomogeneous dose distribution and provides weighted dose values which are inherently inclusive of biological information. Since the output from this approach is still in the dose domain, it is more easily accepted, whereas the models used to calculate EUD can vary based on formalism describing dose-response of different tumor types. The other approach in

BGRT directly focuses on the main objectives of radiation therapy: maximizing tumor control probability (TCP) and minimizing normal tissue complication probability (NTCP).

The concept of equivalent uniform dose (EUD) was originally proposed by Niemierko [19]. The premise is the same as the previously introduced effective dose which is to use one single dose value to describe the biological effect of an inhomogeneous dose distribution. Based on radiobiological data, including survival fraction after 2Gy (SF_2) and α/β, EUD is designed to give the same tumor cell survival fraction as the inhomogeneous dose distribution will give. Dose fractionation, α/β and, if necessary, inhomogeneous tumor cell density, can be all taken into account. Sometimes, effective dose is also regarded as equivalent to EUD, i.e., these two terms can be used interchangeably.

$$EUD = \frac{N_f}{2} \cdot \left[-\frac{\alpha}{\beta} + \sqrt{\left(\frac{\alpha}{\beta}\right)^2 + 4 \cdot \frac{D_{ref}}{N_f} \cdot \left(\frac{\alpha}{\beta} + D_{ref}\right) \cdot \frac{\ln A}{\ln SF_2}} \right]$$

$$\text{whereas, } A = \sum_{i=1}^{N} V_i \cdot \rho_i \cdot (SF_2)^{\frac{D_i}{D_{ref}} \cdot \frac{\alpha/\beta + D_i/N_f}{\alpha/\beta + D_{ref}}} \Big/ \sum_{i=1}^{N} V_i \cdot \rho_i \qquad (1.13)$$

Here, SF_2 is cell surviving fraction after 2Gy. V_i, ρ_i are the volume and cell density of each voxel respectively. N_f is the total number of fractions. D_{ref} is usually set to 2Gy. An objective function based on the EUD is proposed by Wu et al in 2002 [20]

$$f_i = \begin{cases} \left[1 + \left(\frac{EUD_0}{EUD}\right)^{\gamma_i}\right]^{-1}, \text{for tumor} \\ \left[1 + \left(\frac{EUD}{EUD_0}\right)^{\gamma_i}\right]^{-1}, \text{for normal tissue} \end{cases} \qquad (1.14)$$

$$F = \prod_i f_i$$

EUD_0 is the prescribed equivalent uniform dose for i^{th} structure, EUD is calculated from the current dose distribution. γ_i is the weight of each organ. In this way the entire DVHs are accounted for in the objective function whereas in the least square function, only certain points of DVH are used. EUD for normal tissue is usually replaced with effective dose (D_{eff}) which further incorporates volumetric response into the optimization. The merit of this objective function is that, F will approach unity only when EUD of target approaches infinity and EUD of normal tissue equals to zero. In other words, the optimization algorithm will keep searching the solution space for a better plan even if all the constraints are met, whereas in least square like objective function, F approaches zero once volume constraints are met. In the latter case, optimization algorithm will "believe" the current solution is the best even though the room for further plan improvement still exists.

The TCP/NTCP approach directly aims at tumor control and normal tissue complication probabilities, which is in contrast to biologically-weighted dose approachs. Poisson statistics is used to develop the mechanistic TCP model:

$$TCP = e^{-N_s} \quad (1.15)$$

where N_s is the number of surviving cells:

$$N_s = N_0 \cdot SF = \sum_i v_i \rho_i SF_i \quad (1.16)$$

Using LQ Model from Eq. 1.5 and taking clonogen repopulation into account:

$$SF = e^{\lambda(T-T_k)} e^{-\alpha D - \beta d D} \quad (1.17)$$

where T is treatment time, T_k is assumed to be the lag between treatment time and accelerated clonogen repopulation. Obviously T-T_k is set to zero if T_k>T. λ is related to tumor potential doubling time, T_{pot}:

$$\lambda = \ln 2 / T_{pot} \quad (1.18)$$

The commonly used TCP formulation can be given out by:

$$TCP = e^{-N_0 \exp[-\alpha D - \beta d D + \lambda (T - T_k)]} \quad (1.19)$$

where N_0 is the initial number of clonogens.

A popular phenomenological model to describe dose-volume dependence for NTCP, Lyman-Kutcher-Burman (LKB) model, was proposed by Lyman et al [21] [22]. It uses three parameters to calculate normal tissue complication probability of a tissue irradiated with partial uniform dose. This model can be readily combined with the concept of EUD or effective dose [22], the NTCP formula for non-uniform dose distribution converted to effective dose D_{eff} (Eq 1.8) is:

$$NTCP(gEUD) = \frac{1}{\sqrt{2\pi}} \int_{-\infty}^{t} \exp(-u^2/2) du \quad (1.20)$$
$$t = (gEUD - D_{50}) / (D_{50} m)$$

Generalized EUD (gEUD) is equal to effective dose D_{eff}. D_{50} is the whole organ dose which will cause 50% of patients to develop complications, m is the parameter describing the slope of dose-response.

The sigmoid function can also be used to describe whole volume dose response [23]:

$$NTCP = \frac{1}{1 + \left(\frac{D_{50}}{D} \right)^{4\gamma_{50}}} \quad (1.21)$$

$$TCP = \frac{1}{1 + \left(\frac{D_{50}}{D} \right)^{4\gamma_{50}}} \quad (1.22)$$

where γ_{50} is the normalized slope of the dose-response curve at D_{50}

$$\left(\left. \frac{dTCP}{dD} \right|_{D_{50}} \right) \cdot D_{50} = \gamma_{50} \quad (1.23)$$

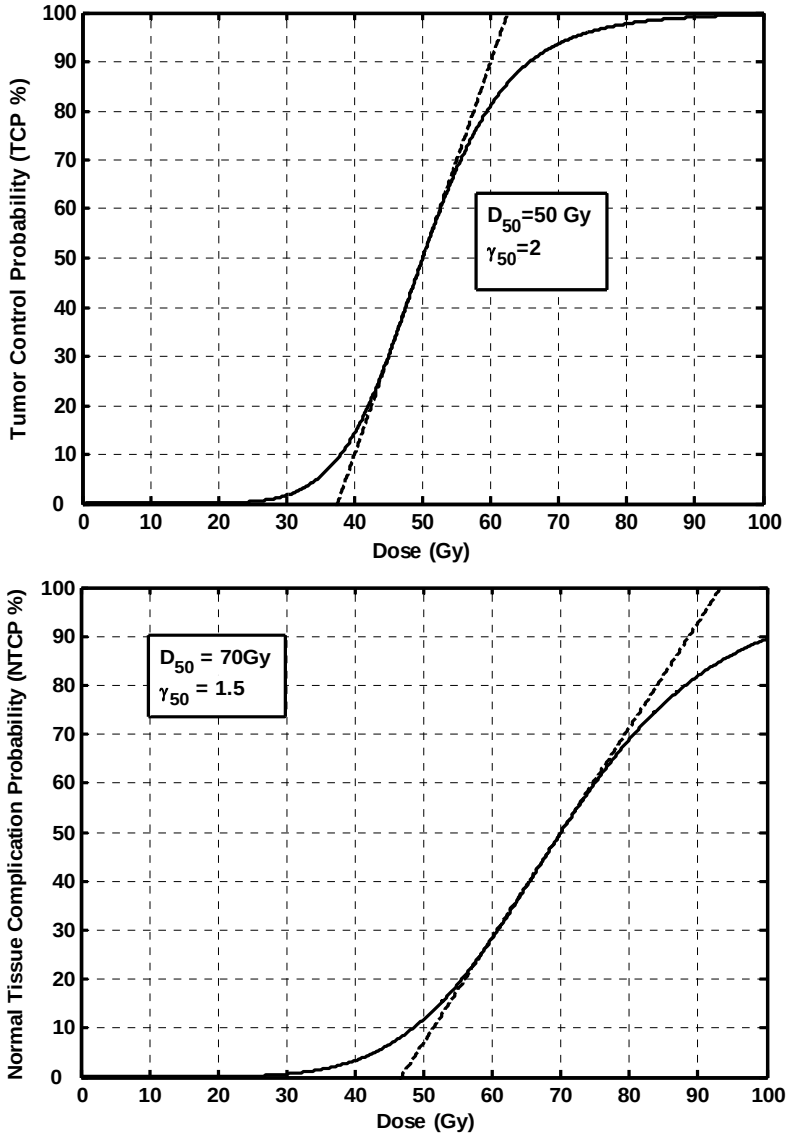

Figure 1.11: Sample TCP (top) and NTCP (bottom) curve. Dashed straight lines indicate the tangential lines at D_{50}

Based on TCP and NTCP, the objective function to achieve complication free radiation therapy [24] or UTCP [25]can be calculated by:

$$UTCP_{\delta} = \left(TCP - NTCP\right) + \delta\left(NTCP\left(1 - TCP\right)\right) \quad (1.24)$$

where δ is the estimated correlation factor, This factor indicates the fraction of patients who have statistically independent tumor and normal tissue response.

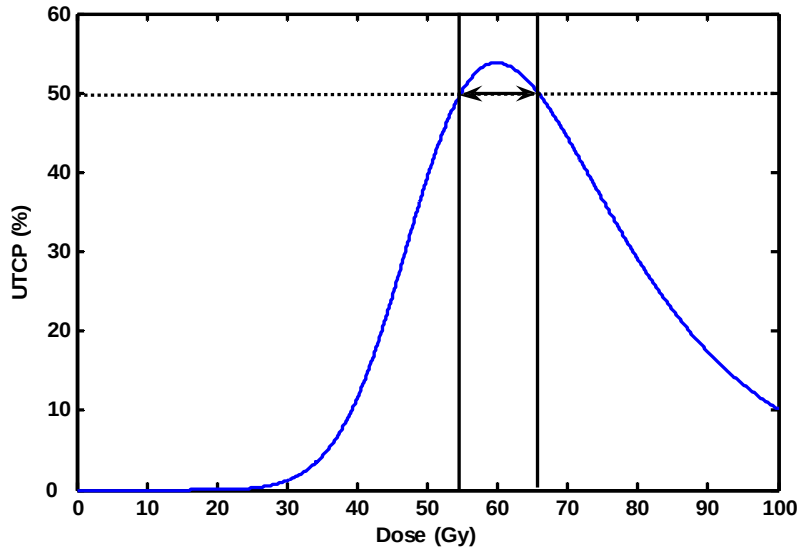

Figure 1.12 Sample UTCP curve calculated from Figure 1.11 assuming δ =0.2

As shown in Figure 1.12, dose between 55Gy to 65Gy will give the patient more than 50% chance to curve the cancer without complication. An ideal treatment plan will have a unity $UTCP_{\delta}$, i.e the patients will have their cancer cured without any complication.

1.4.3. Volumetric Modulated Arc Therapy (VMAT)

Volumetric Modulated Arc Therapy (VMAT) [26] is a novel dose delivery technique developed by Dr. Karl Otto for Intensity Modulated Radiation Therapy (IMRT). Compared to conventional dose delivery techniques which deliver dose from a number of gantry angles, the unique feature of VMAT is that the entire fraction can be delivered in a single gantry rotation with multileaf collimator moving during the gantry rotation thereby providing a continuous intensity modulation. Since dose is delivered from 360 degrees, VMAT would produce tighter dose coverage of target volumes while efficiently sparing

normal tissues. With multileaf collimator moving during the dose delivery and dose delivered in a single gantry rotation, the delivery time for each fraction is reduced from ~10-15 minutes in 5-9 field IMRT to ~2 minutes. Dose delivery with VMAT also requires substantially less monitor units (MU), compared to 5-9 field IMRT. This reduction in MU also significantly reduces dose leakage and transmission through the multileaf collimator thus minimizing the chance of secondary cancer introduced by IMRT [27]. In Figure 1.13, is the field set-up for a head & neck cancer patient with dose delivered through entire gantry rotation from all 360 degrees. On the bottom is the enlarged figure of multileaf collimator set-up. It can be seen that the shape of multileaf collimator keeps changing during the gantry rotation.

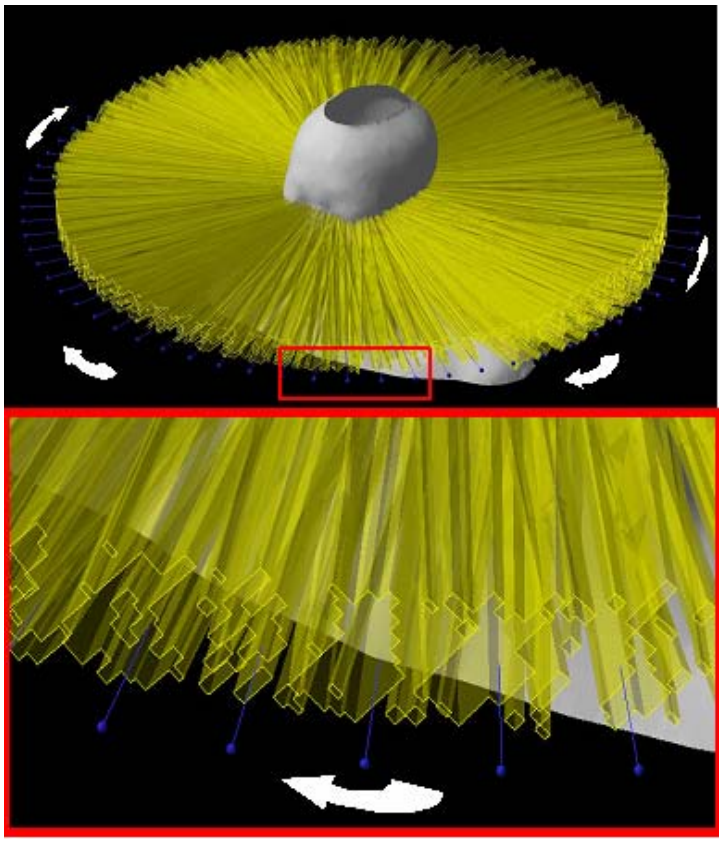

Figure 1.13 Illustration of VMAT‘s technical feature. (Courtesy Dr Karl. Otto)

The in-house VMAT treatment planning program MonArc was used as the primary treatment planning program for the projects in this thesis unless specified otherwise.

CHAPTER 2. Biological Optimization of Prostate Cancer with Tumor Hypoxia: Dose Painting and Urethra Sparing

2.1. Mechanisms of Cell Hypoxia and Its Effect

Free radicals play an important role in the chain of events from absorption of radiation to expression of biological damage. Breakages of DNA molecule chemical bonds brought about by free radicals ultimately result in DNA damage leading to cell transformation or death. In the absence of oxygen, DNA reacts with free radicals (R·). The produced damage can be chemically restored through reaction with a SH group, whereas in the presence of oxygen DNA can react with chemical species derived from oxygen (RO_2·), resulting in the DNA radicals which are non-restorable. This is known as the *oxygen fixation hypothesis*, i.e. the damage of chemical bonds can be "fixed" by oxygen, making the repair mechanisms of DNA less effective. In hypoxic cells, the repair process is more effective which means cells are more resistant to radiation.

Effect of presence of oxygen on mammalian cell survival following irradiation with X-rays has been observed in numerous experimental studies. Formalism to numerically describe oxygen effect was subsequently suggested [1]. The ratio of dose needed to achieve equivalent effect (e.g., cell survival) in the presence and absence of oxygen is defined as the oxygen enhancement ratio, OER. The OER value is related to the type of radiation. It is unity for low-energy α particles, whereas it is ~2.5 for a variety of cell lines irradiated with X-rays [1].

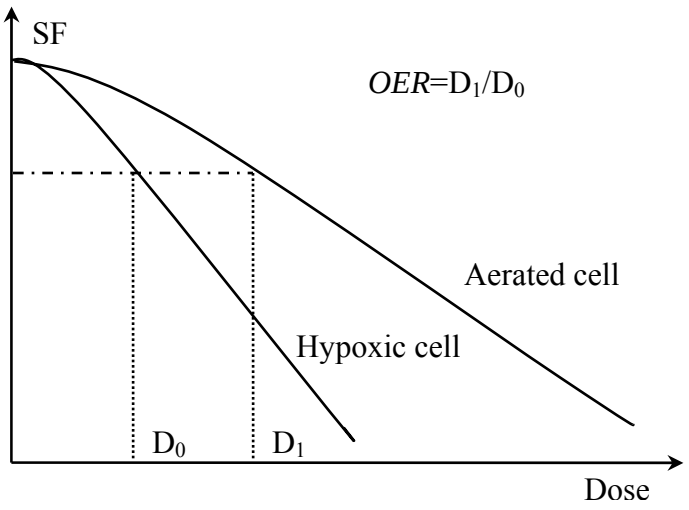

Figure 2.1: Survival curves of mammalian cells irradiated with X-rays in the presence and absence of oxygen.

While in experimental studies of cell survival *in vitro* oxygen concentration is typically uniform through the dimensions of a specimen, *in vivo* oxygen partial pressure varies spatially within a tumor. It also changes as radiation therapy progresses. Partial hypoxia is caused by the limited oxygen diffusion through stroma (i.e., tissues not directly responsible for organ function, for example connective tissues) or from blood vessels to tumor cells. Tumor hypoxia is highly spatially heterogeneous, typically the core exhibits the most pronounced hypoxia because of severely compromised perfusion and oxygen diffusion. As demonstrated in Figure 2.2, irradiating this mixed colony with a hypoxic core with a modest dose will result in preferential killing of most aerated cells whereas most hypoxic cells will survive. If sufficient time is allowed before next fraction, the remaining hypoxic cells will become partially oxygenated, irradiation at this time will therefore result in efficient inactivation of previously hypoxic, but now re-oxygenated cells. If this process is repeated several times, entire cell colonies can be gradually depleted, despite the enhanced resistance caused by hypoxic cells.

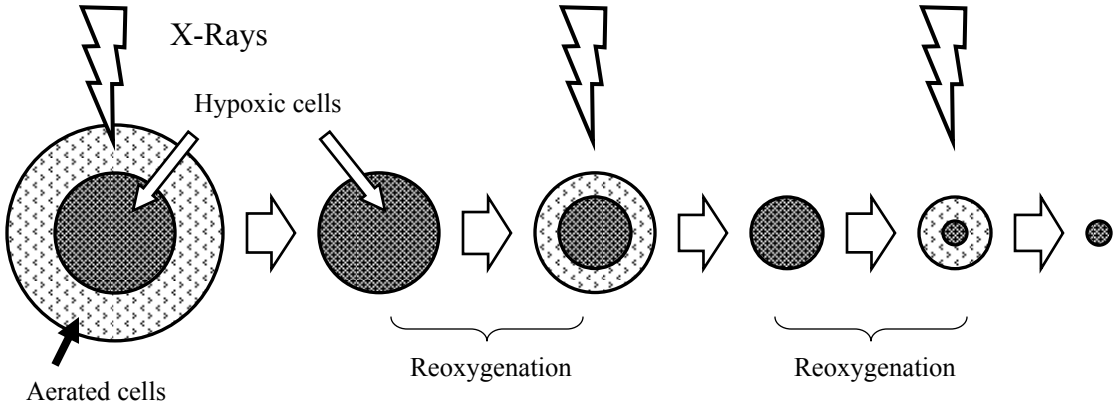

Figure 2.2: Illustration of re-oxygenation.

The implication of re-oxygenation is that, if human tumor cells are re-oxygenated as expected, a multi-fraction treatment schedule extended over a period of time will be an effective means to inactivate hypoxic tumor cells. An important conclusion from *in-vivo* experiment is that the proportion of hypoxic cells remains almost constant after each re-oxygenation [1].

2.1.1. Chronic Hypoxia and Acute Hypoxia

Two different types of hypoxia are observed based on their oxygenation patterns. Chronic hypoxia (*ch*-) is the result of limited vascular oxygen diffusion ability inside the tumor which can be revealed by direct *in vivo* electrode measurements [28-30]. *In vivo* measurement of human and murine tumor blood flow suggests that acute hypoxia is also common in tumors [31]. Mechanistic interpretation of the acute hypoxia (*ah*-) is that tumor blood vessels randomly close and open, which is the cause of intermittent hypoxia, i.e., acute hypoxia.

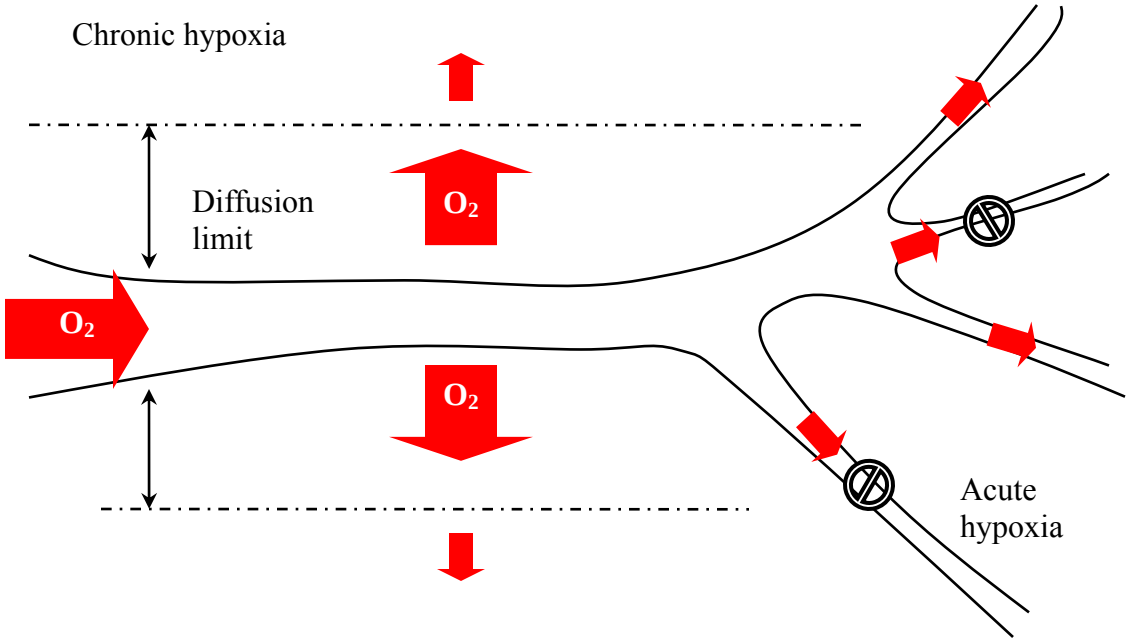

Figure 2.3: Mechanisms of chronic and acute hypoxia

As shown in the Figure 2.3, the distance of oxygen diffusion is limited in the tumor. This distance is mainly dependent on the metabolism rate of respiring tumor cells. A rapidly respiring cell consumes most of the diffused oxygen, whereas tumor cells beyond the diffusion range remain hypoxic for a long period of time. In contrast, acute hypoxia is caused by random opening of malformed blood vessel. Permanently closed blood vessel will result in necrosis of cells downstream, however randomly open/closed blood vessels will result in intermittent tumor hypoxia.

2.1.2. The Effect of Tumor Hypoxia in EBRT for Prostate Cancer

The effect of hypoxia has been particularly emphasized because of its well established radiobiological basis [1] and relevance to radiation therapy (RT) of cancer. Presence of hypoxic regions in prostate cancer has been demonstrated by direct *in vivo* measurements of oxygen tension [28-30].

Clinical studies on head & neck cancer and prostate cancer have suggested that tumor hypoxia will adversely affect the clinical outcome after RT [32-34]. Currently used dose prescriptions (70Gy in 2Gy/fr) for external beam radiation therapy (EBRT) is insufficient to provide optimum tumor control probability (TCP) [34]. Dose boosting would therefore be required to overcome tumor hypoxia.

2.2. Unconstrained Biological Optimization Using Hypoxia Model

2.2.1. Background

The high dose gradient achievable with Intensity-modulated radiation therapy (IMRT) provides the ability to deliver a heterogeneous dose distribution addressing spatial inhomogeneity of tumor response which has led to the creation of the "dose painting" concept. Practical application of the concept of dose painting has been receiving growing support as imaging modalities progressed towards mapping biological characteristics of tumors beyond hypoxia [24,25,35-38]. Recent achievements of medical imaging techniques including positron emission tomography (PET), single photon emission computed tomography (SPECT) and magnetic resonance spectroscopy imaging (MRSI) have provided non-invasive imaging methods to map clonogen density and tumor proliferation rate in addition to hypoxia. IMRT or 3D conformal RT (3D CRT) plans accounting for these biological characteristics have been shown to be feasible [35][24]. Recently published planning studies [24,25,35] demonstrated how biologically guided RT (BGRT) plans can achieve dose boosts inside prostate while effectively sparing normal tissues outside of prostate.

One of the potentially limiting factors for these boosts is dose to urethra. Current RT protocols do not include urethra in EBRT planning due to lack of reliable methods to visualize it on CT images. However, surrogate volumes can be used to estimate urethra dose. The comparison between dose in the urinary catheter and simple deviated surrogate by Bucci et al [39] suggests that a simpler derived surrogate is suitable for clinical practice as it provides close correlation on dose-volume indices of urethra. MRI studies by McLaughlin et al [40] also show that although internal sphincter might not be clearly visible as a result from transition zone hypertrophy, external sphincter, including membranous urethra sphincter and prostatic sphincter, are clearly visible on T2 weighted MRI. This result demonstrated the feasibility of identifying some peri-urethral structures, therefore providing the opportunity to contour urethra in RT planning. Dose correlation of genito-urinary toxicity with dose-volume parameters for bladder and urethra has not been fully resolved. Urinary incontinence has been reported as a rare incidence in patients who received less than 78Gy in definitive EBRT without prostatectomy [41-43]. However, urinary response at higher dose (>80Gy) is still unclear and dose up to 100Gy might occur in prostate in some of our plans, thus we incorporate urethra into planning.

2.2.2. Materials and Methods

CT scans of 25 prostate cancer patients who recently received radiation therapy at the British Columbia Cancer Agency (BCCA) were selected. Of these 25 patients 22 were treated with 3D CRT and 3 with 5-field IMRT. Patients were selected to cover a broad range of Ant/Post and lateral separations, as well as prostate, rectum and bladder volumes (Table 2.1). Rectum, bladder and femoral heads were contoured by a dosimetrist, contours were approved by a treating radiation oncologist. Clinical target volume (CTV)

defined as “prostate only” was contoured by a treating oncologist. For 3D CRT patients, planning target volumes (PTV) were obtained from CTV by adding a uniform 1cm margin in three dimensions, with posterior margin further adjusted at the physician’s discretion. According to BCCA protocol, prostate IMRT patients are implanted with gold fiducial markers for realignment using EPI. PTV margins for these patients were set to 0.5 cm in posterior dimension and 0.75 cm in all other dimensions.

Table 2.1 Range of organ volumes in selected patients (cm^3)

	CTV	PTV	Rectum	Bladder
Min	14.0	71.6	35.2	89.6
Mean	45.0	162.3	81.2	329.4
Max	91.0	278.4	147.6	659.8

Urethra contours were drawn by a radiation oncologist (the urethra was not visible on the planning CT scan, but the position was approximated from anatomy references) while hypoxic regions were randomly added on CT scans. The manner in which these hypoxic regions were contoured is illustrated in Figure 2.4. Two hypoxic regions (chronic and acute) were confined to CTV only and not overlapping with urethra. While locations of these hypoxic areas were selected randomly for each CT scan, overall all possible locations were covered. Approximately 20% of CTV volume was designated as chronic hypoxia region, PTV_Ch. This 20% chronic hypoxic fraction is consistent with both theoretical simulation results [44] and *in vivo* molecular imaging studies by H.Yuan et al [45]. In the latter study it was demonstrated that approximately 20% of tumor cells were marked as chronic hypoxic in R3230 mammary adeno-carcinomas (R3230Ac) and 9L gliomas(9L) cells.

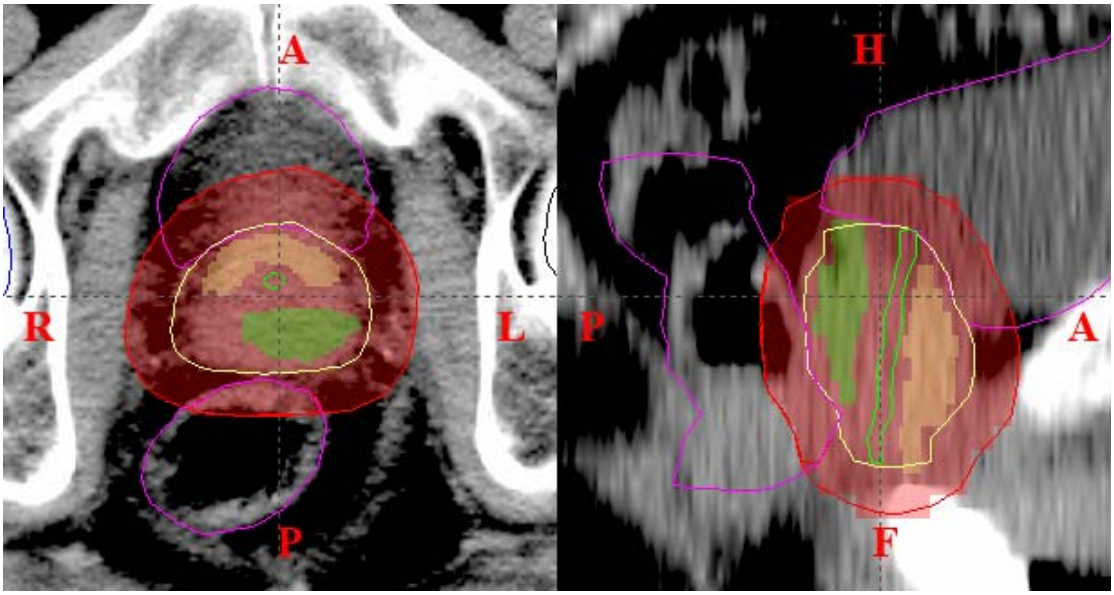

Figure 2.4 Transversal (left) and sagittal (right) view of structure contours in CT image (patient #1). Green contour shows urethra. Yellow contour in the center is CTV with chronic hypoxia region (yellow segment) and acute hypoxia region (green segment).

The acute hypoxia data from *in vivo* pO_2 measurements in prostate cancer are inconclusive. In this study, 15% of the CTV was designated as an acute hypoxia region, PTV_Ah. In reality, acute hypoxic volumes are usually discretely distributed, thus we assumed that not all the cells inside PTV_Ah are acute hypoxic. Only 70% of all the voxels inside the PTV_Ah volume were randomly chosen as acute hypoxic. This means that roughly 10% of cells in the CTV are truly acutely hypoxic. The period of a complete pO_2 cycle was set to 10 minutes which was adapted from pO_2 record with periodical minimum value approximately every 10 minutes in the study of oxygenation fluctuation [46]. Acutely hypoxic cells were assumed to spend 60% of the time in the hypoxic state on average which is consistent with in vivo measurement of intermittent hypoxia (pO_2<5mmHg) in R3230AC tumors [31]. The remaining area in the PTV was designated as PTV_Ox (oxygenated region). All the tumors cells in PTV_Ox and 30% of cells in

PTV_Ah were considered well oxygenated throughout the treatment.

The radiobiological parameters of oxygenated and hypoxic tumor cells were adapted from those reported by Nahum et al [7] where averages of various human prostate cancer cell lines were presented. For oxygenated cells surviving fraction after 2Gy, SF2, was set to 0.5248 [47]. Based on linear quadric (LQ) model,

$$SF = \exp(-\alpha D - \beta D^2) \quad (2.1)$$

one can readily derive α and β as an function of SF2 and α/β.

$$\alpha_{aerobic} = \frac{-\ln SF2}{2 + 4(\alpha/\beta)^{-1}}$$
$$\beta_{aerobic} = \frac{-\ln SF2}{2(\alpha/\beta) + 4} \quad (2.2)$$

OER_α =1.75 and OER_β=3.25 [7] were used to correct both α and β terms of the LQ expression for presence of hypoxia:

$$OER_\alpha = \alpha_{aerobic} / \alpha_{hypoxic}$$
$$OER_\beta = \sqrt{\beta_{aerobic} / \beta_{hypoxic}} \quad (2.3)$$

During the last several years there have been debates over the α/β ratio for prostate cancer cells [7,9,47,48]. From the above equations a combination of SF2 for oxygenated cells and pre-set value of α/β uniquely defines LQ parameters α and β. In this study, α/β of 8.33Gy and 1.5Gy for oxygenated cells were used to address the uncertainty in its value. Above shown OER values were applied to account for hypoxia irrespective of α/β values. Sets of radiobiological parameters are shown in Table 2.2. Twenty five treatment plans were generated using biological parameters in Table 2.2 Set I (α/β=8.33Gy). Three treatment plans were also generated using parameters in Table 2.2 Set II (α/β=1.5Gy).

Table 2.2 Radiobiological parameters used in this model.

	Set I (α/β=8.33Gy)	Set II (α/β=1.5Gy)

	Oxygenated cells	Hypoxic Cells	Oxygenated cells	Hypoxic Cells
SF2	0.5248	0.7342	0.5248	0.8246
α (Gy^{-1})	0.26	0.1486	0.1382	0.0790
β (Gy^{-2})	0.0312	$2.95x10^{-3}$	0.0921	$8.72x10^{-3}$
α/β (Gy)	8.33	50.2976	1.5	9.056

Plan optimization was based on delivering the total dose in 35 fractions. The dose per fraction in the *i*th voxel d_i is:

$$d_i = D_i / n \quad (2.4)$$

where n is the number of fractions. Note that in unconstrained optimization, acute hypoxia cells and chronic hypoxia cells would receive more than 70Gy, thus d_i is variable between voxels and it is usually more than 2Gy/fr for dose boosting regions. Doses in voxels occupied by target volumes and normal tissues were converted to normalized total dose (NTD), i.e., isoeffective dose in 2Gy/fr:

$$NTD_i = D_i \frac{\alpha/\beta + d_i}{\alpha/\beta + 2\text{Gy/fr}} \quad (2.5)$$

where D_i is the dose delivered to voxel i in 35 fractions. Value of α/β was set to 3Gy for all normal tissues except urethra (we assumed that *NTD* equals total Dose for urethra here) since there are insufficient supporting studies.

2.2.3. Hypoxia Model

The model proposed by Ruggieri and Nahum [49] was incorporated into optimization with some modifications. This model accounts for the effects of both acute hypoxia and chronic hypoxia. In this study we further assumed that for chronic hypoxia re-oxygenation does not occur until the end of the 7th fraction. This assumption was based

on clinical observation [32] suggesting that re-oxygenation is not observed before 10-15Gy in 2-2.5Gy/fr for head and neck cancer patients. Tumor cell density was assumed to be uniform inside the PTV. The latter assumption, while not reflecting the realistic spatial distribution of tumor cells, is used for optimization purposes only. Overall tumor cell surviving fraction can be described as:

$$SF = (1 - AHF - CHF) \times SF^{ox} + AHF \times SF^{ah} + CHF \times SF^{ch} \quad (2.6)$$

AHF, CHF are pre-treatment fraction of *ah-, ch-* cells in PTV. SF^{ox}, SF^{ah}, SF^{ch} are defined as the number of surviving *ox-, ah-, ch-* cells divided by the number of pre-treatment *ox-, ah-, ch-* cells respectively.

Surviving fraction for oxygenated cells.

It is convenient to calculate tumor cell survival fraction using SF2 for oxygenated cells:

$$SF^{ox} = \frac{1}{N_{ox}} \sum_{i=1}^{N_{ox}} (SF_2^{ox})^{NTD_i / 2} \quad (2.7)$$

N_{ox} is the number of voxels inside the PTV_Ox region.

Surviving fraction for chronic hypoxia cells.

The inactivation of *ch-* cells is modeled as a fully structured process: a certain fraction of *ch-* cells are re-oxygenated after each fraction. Brizel et al [32] reported that tumor oxygen level after 10-15Gy was unchanged compared to the pretreatment level in H&N cancer patients. We applied this assumption for the purposes of this study. Another assumption is that the time when re-oxygenation starts mainly depends on the number of fractions delivered, thus we assume that re-oxygenation will start after the 7th fraction

regardless of its size. Therefore *ch*- cell survival can be expressed as:

$$SF_i^{ch} = \begin{cases} \left(SF_2^{ch}\right)^{NTD_i/2} \text{ less than 7 fractions} \\ \left\{ \sum_{j=1}^{n} \left[B(1-B)^{j-7} \left(SF_2^{ch}\right)^{(j-7)\times d_i/2} \left(SF_2^{ox}\right)^{(NTD_i - j\times d_i)/2} \right] + (1-B)^{n-6} \left(SF_2^{ch}\right)^{(NTD_i - 7\times d_i)/2} \right\} \times \\ \left(SF_2^{ch}\right)^{7\times d_i/2} \text{ more than 7 fractions} \end{cases}$$

(2.8)

Note that the number of fractions was set to 35. *B* is the ratio of re-oxygenation after each fraction. It was set to 0.1 throughout the optimization, i.e. 10% of the surviving *ch*-cell are re-oxygenated before the next fraction.

Surviving fraction for acute hypoxia cells.

Acute hypoxia in CTV is caused by random opening/closing patterns of blood vessels. As was mentioned above, the period of a complete pO_2 cycle was set to 10 minutes for each cell and all the cells in each voxel were assumed to spend on average 60% of the time in the hypoxic state. Before optimization starts, a random starting point in this oxygenation cycle during different fraction is assigned to each ah-voxel. F_{ij}, the oxygenated time, can be calculated from the patterns of the pO_2 cycle and the dose delivery time for one fraction set to 2 minutes for VMAT. The survival fraction can be calculated from

$$SF^{ah} = \prod_{j=1}^{n} \left\{ \frac{1}{N_{ah}} \sum_{i=1}^{N_{ah}} \left[\left(SF_2^{ox}\right)^{F_{ij}\times d/2} \times \left(SF_2^{ah}\right)^{(1-F_{ij})\times d/2} \right] \right\} \quad (2.9)$$

where F_{ij} is the ratio of oxygenated time of tumor cell in *i*th voxel during the *j*th fraction.

2.2.4. Optimization Method and Parameters

We adapted the unconstrained objective function proposed by Wu et al [20]. Equivalent Uniform Dose (EUD) [19] was used as a suitable surrogate for outcome to optimize and evaluate treatment plans. The main problem with unconstrained biologically-based optimization is that it leads to clinically unacceptable hot stops in PTV. To avoid this we introduced a dose inhomogeneity control factor. The objective function for unconstrained biologically-based optimization was formulated as:

$$F = \prod_i f_i \times f_h^{ox} \times f_h^{ah} \times f_h^{ch} \quad (2.10)$$

$$f_i = \begin{cases} \left[1 + \left(\frac{EUD_0}{EUD}\right)^{\gamma_i}\right]^{-1}, \text{for tumor} \\ \left[1 + \left(\frac{EUD}{EUD_0}\right)^{\gamma_i}\right]^{-1}, \text{for normal tissue} \end{cases} \quad (2.11)$$

where f_h^{ox}, f_h^{ah} and f_h^{ch} are dose inhomogeneity control factors which will be explained later. In Eq.2.11, EUD is the calculated equivalent uniform dose in the optimization; EUD_0 is the desired equivalent uniform dose and γ_i is the priority for each organ. The parameters used in the optimization are shown in Table 2.3. For a perfect treatment plan, F will approach unity.

Table 2.3 Optimization Parameters used in Eq.2.11 and Eq.2.12

	n (Burman et al [13])	EUD_0 (Gy)	γ
Bladder	0.5	65	5
Femoral Head	0.25	52	5
Rectum	0.12	65-70	15
Urethra	0.06	70	15
PTV	-	80	20

For normal tissue, EUD is described by

$$EUD_{OAR} = \left(\frac{1}{N_{OAR}} \sum_{i=1}^{N_{OAR}} D_i^{1/n} \right)^n \quad (2.12)$$

N_{OAR} is the number of voxels in the organ at risk (OAR). n is the parameter from the LKB model [13]. Urethra was assumed to respond to radiation in the same manner as esophagus, i.e. n=0.06. EUD_0 was set equal to $TD_{5/5}$ for bladder and femoral heads [50]. For rectum and urethra, EUD_0 was selected on a trial-and-error process. We found that 65-70Gy for rectum and 70Gy for urethra provide treatment plans with rectum and urethra sparing as well as dose volume histograms (DVH) which were acceptable for treatment as judged by a radiation oncologist and compliant with recommended treatment planning guidelines [11,50].

For the target volume, EUD was derived from a pre-calculated EUD-SF table. Before optimization starts a patient-specific Dose-Surviving fraction table was pre-calculated based on Eq.2.6- Eq.2.9 assuming a uniform dose in the range 0-120Gy delivered to PTV. Because the dose in this calculation is equal in every target voxel, this table is the EUD-SF table by definition. During the optimization, tumor cell surviving fraction from a non-uniform dose distribution is calculated on a voxel by voxel basis followed by summation over all voxels. The corresponding target EUD could be readily obtained from the pre-calculated EUD-SF table.

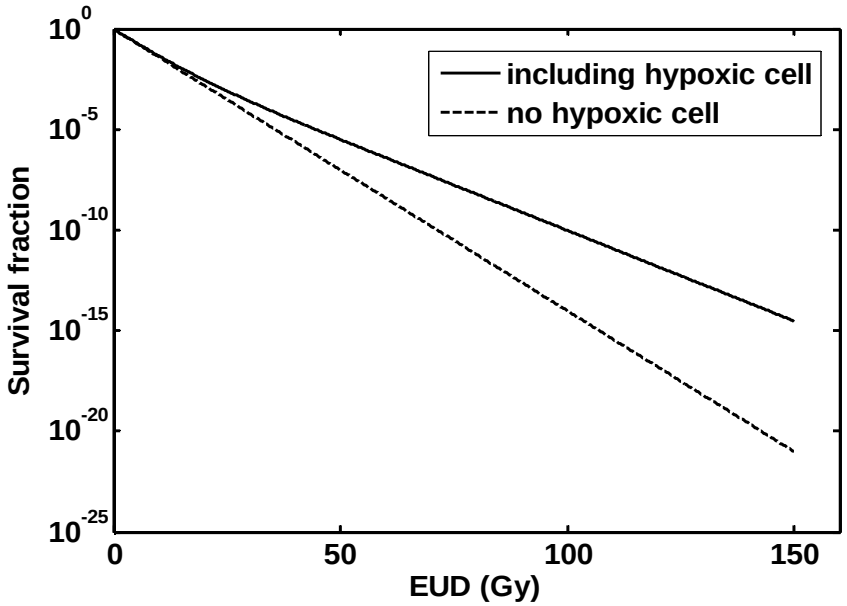

Figure 2.5: EUD-SF graph

From our experience in this study, if no attempt is made to control dose inhomogeneity during the EUD based optimization, hot spots will occur in target volume. This was also shown in the study by Wu et al [20]. To avoid this, we introduced a new factor f_h which is shown in Eq.2.10, to control dose inhomogeneity in a reasonable range.

$$f_h = \frac{1}{1+\left(\frac{\mathrm{std}(D_i)/\overline{D_i}}{\mu}\right)^{\gamma}} \quad (2.13)$$

In this equation, μ is acceptable dose inhomogeneity; $std(D_i)$ is standard deviation of dose arrays D_i of a particular target region. This factor is applied to acute hypoxia, chronic hypoxia and oxygenated parts of PTV separately to achieve clinically acceptable dose inhomogeneity in specific target volumes. Oxygenated and hypoxic areas were assigned different μ values and priorities, γ, because a uniform dose distribution is favored in oxygenated area while some dose inhomogeneity should be allowed in

hypoxic area. This approach will tend to minimize dose inhomogeneity, however because f_h does not vary a lot when dose inhomogeneity is considerably smaller than pre-set μ, it allows certain acceptable dose inhomogeneity to balance between physical conformality and biological conformality. These dose inhomogeneity control parameters are shown in Table 2.4

Table 2.4 Dose inhomogeneity control parameters used in Eq.2.13

	Tolerable dose inhomogeneity (μ)	Priority (γ)
Oxygenated area	5%	7
Acute hypoxia area	10%	5
Chronic hypoxia area	10%	5

2.3. Results

Biologically optimized VMAT plans were generated for all twenty five patients with α/β for prostate cancer cells set to 8.33Gy. Obtained EUD values for PTV and normal tissues are listed in Table 2.5. Also shown in the table are EUD values obtained for a typical treatment plan for Patient#1. This plan will be used for further illustrations below.

Table 2.5. EUD(Gy) and volume (cm3) for different organs

	Min (Gy)	Mean (Gy)	Max (Gy)	Patient #1 (Gy)	Volume (cm^3,Patient #1)
PTV	80.42	83.33	86.94	83.77	143.75
Rectum	53.90	59.47	62.72	60.08	67.78
Urethra	62.85	64.46	66.53	64.47	0.06
Bladder	15.14	31.81	59.14	31.44	264.27
Lt Femoral Head	7.63	14.54	26.29	17.90	177.33
Rt Femoral Head	9.68	14.42	22.55	15.89	182.45

More than 95% of PTV is covered by 70Gy in all the patients. Maximum dose of approximately 100Gy was observed in hypoxic region while minimum dose of 65Gy was observed at the PTV edge. Chronic and acute hypoxia areas received at least 75Gy. Chronic hypoxia cells are generally more radioresistant compared to acutely hypoxic

cells in this model, although this is highly dependent on the value of *B* in Eq.2.8. Thus the chronic hypoxia region usually received larger dose compared to the acute hypoxia region, however in some plans (fewer than 5) dose to acute hypoxic regions is not lower than that to chronic hypoxic regions.

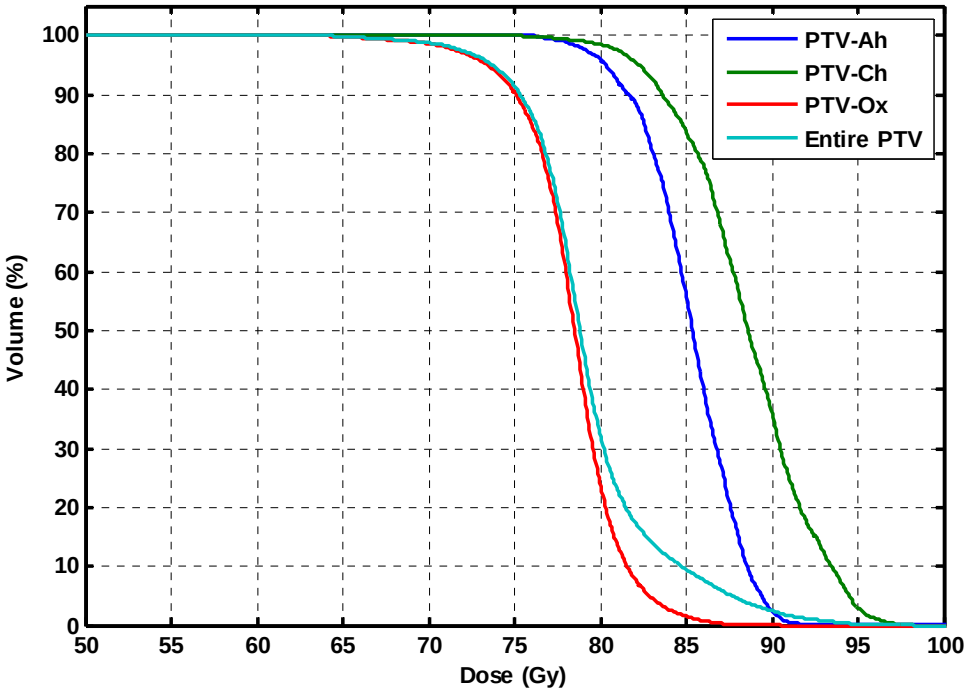

Figure 2.6: Target Dose Volume histograms (patient #1)

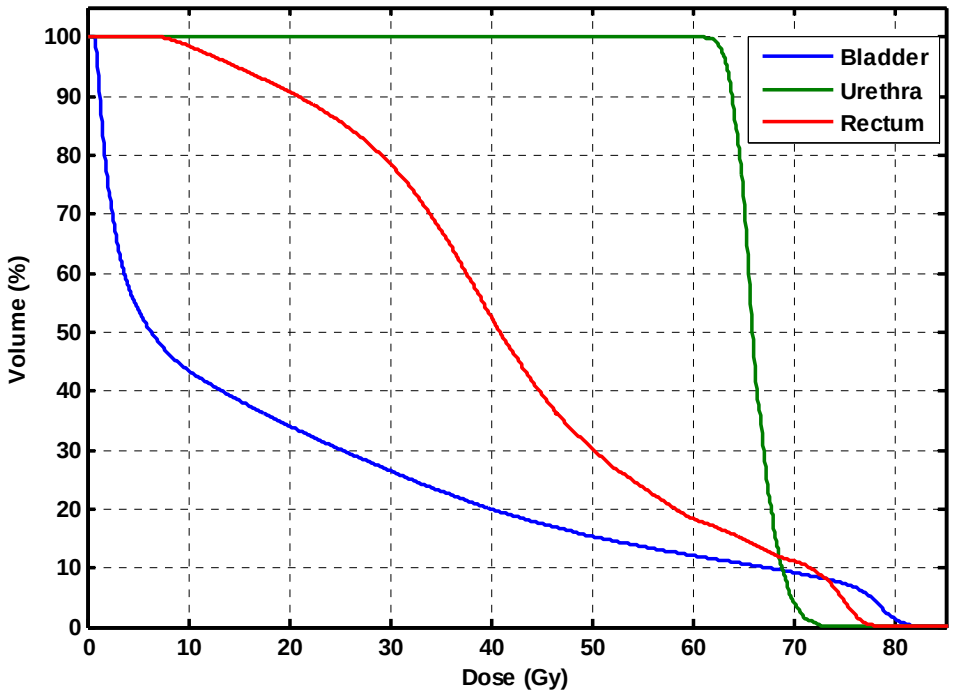

Figure 2.7: Dose Volume Histograms of Normal tissues (patient #1)

All the normal tissues including rectum and urethra were well spared (Figure 2.7 and Figure 2.8). All DVHs complied with constraints used for 3D CRT planning suggested in RTOG 0126 [11]. Specifically, volume receiving at least 70Gy (V70) ranged from 5% to 20% with typical values of approximately 15%. This is well compliant with RTOG0126 constraints requiring that V70<25%. Excellent urethra sparing was achieved in all plans. A relative cold spot closely conforming to urethra is clearly seen in the PTV both in transversal and sagittal planes (Figure 2.8).

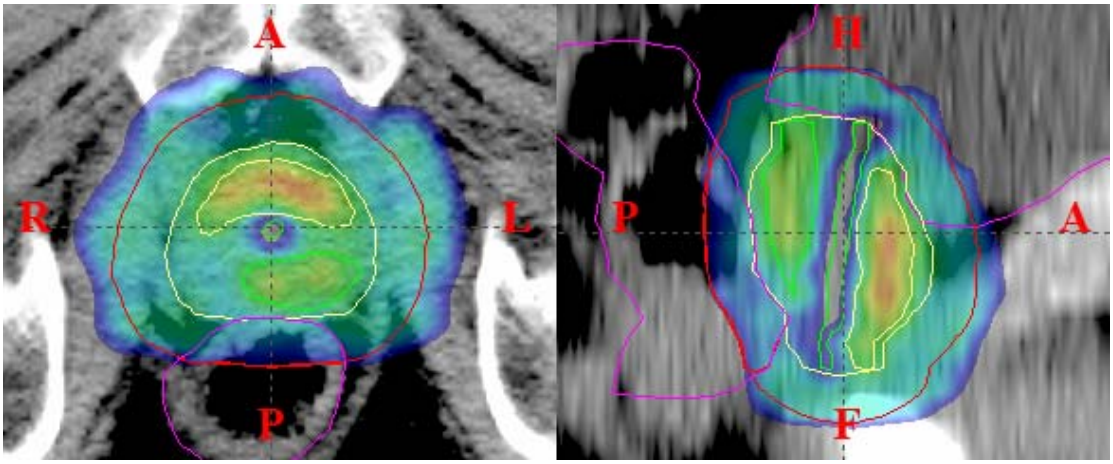

Figure 2.8: Transversal (left panel) and sagittal (right panel) dose distributions for the treatment plan of patient #1. Dose colourmap ranges from 67Gy (blue) to 98.32Gy (red). Chronic hypoxia area is at the anterior part of PTV with acute hypoxic area on the posterior part and urethra between two hypoxic regions.

Sharp dose gradients inside the PTV are further illustrated as a line dose readout Figure 2.9. This line was drawn to go through organs at risk, rectum and bladder, as well as hypoxic areas.

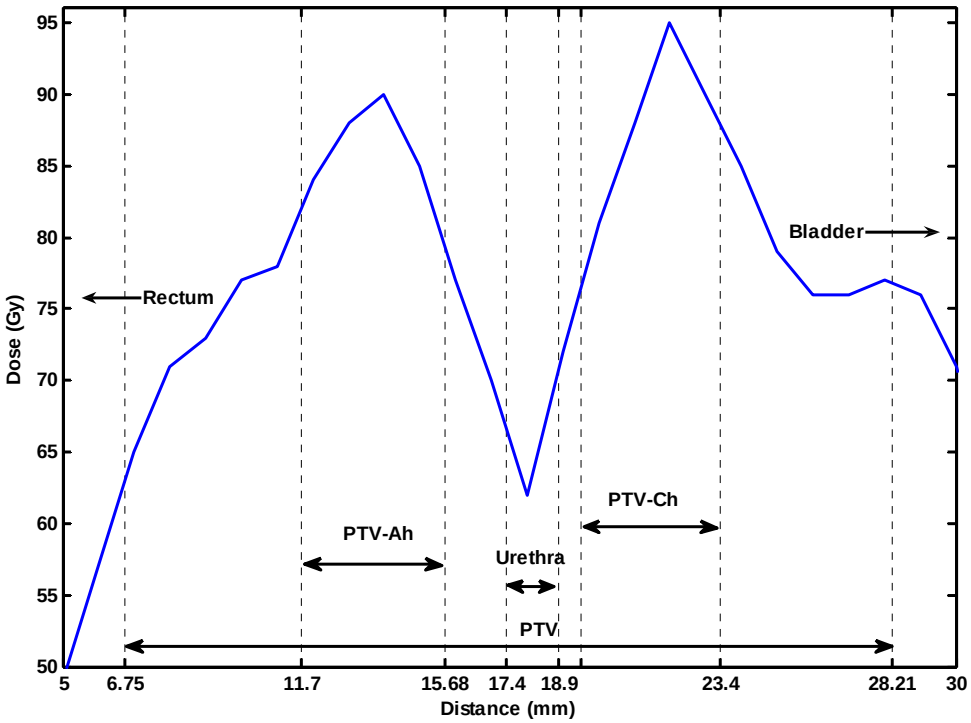

Figure 2.9: Line dose profile along the anterior-posterior axis

Figure 2.9 shows that cold spots in PTV (exclusive of urethra) are mainly located at the boundary between PTV and rectum. Also note that the line dose profile, Figure 2.9, shows that dose corresponding to the anterior aspect of the patient's anatomy (portion of PTV adjacent to bladder) exceeds the dose on the posterior aspect (portion of PTV adjacent to rectum), which suggests that the optimization routine accounts for higher radiosensitivity of rectum compared to bladder. This is likely related to EUD-based biological optimization which automatically determines sparing priorities of different normal tissue based on their *n* parameter in Eq.2.12

2.4. Discussions

2.4.1. Sensitivity to Model Parameter Values

The current limitation of this study is that most of the parameters used in the hypoxia model come from tumor xenografts. However, there is no doubt that these parameters would be available for human prostate tumor using functional imaging in the near future. The question remains whether this biological optimization approach would be still feasible as it is unlikely those parameters from human prostate tumor would be the same as those used in this study. Several tests were conducted to validate the robustness of the proposed approach.

Four tests on three patients' plans were conducted to test the sensitivity of the proposed method to the size of hypoxic volumes.

Table 2.6 Resultant EUD (Gy) of sensitivity test on size of hypoxic volumes

Patient#1	I	II	III	IV	V	Patient#2	I	II	III	IV	V
PTV	83.8	81.8	82.9	81.8	83.5	PTV	82.2	83.0	84.5	83.0	84.3
Rectum	60.1	57.2	56.0	57.6	56.5	Rectum	61.2	60.8	60.0	60.4	59.6
Urethra	64.5	65.4	64.9	65.8	63.2	Urethra	65.2	64.2	62.7	65.0	62.7

	I: original plan
Patient#3	II: PTV_Ch size +50%, PTV_Ah unchanged
PTV	III: PTV_Ch size -50% , PTV_Ah unchanged
Rectum	IV: PTV_Ch unchanged , PTV_Ah size +50%
Urethra	V: PTV_Ch unchanged , PTV_Ah size –50%

Table 2.6 shows that RT plans obtained with the proposed BGRT method show very little sensitivity to size of hypoxic volumes. Using unconstrained optimization, it was possible to obtain dose painting plans with various dose boosting volumes. Note that this is achieved without significant dose increase in urethra which is located in close proximity to dose boosting volumes. Location of hypoxic volumes could be a potential limiting factor. In all the plans, hypoxic volumes were added in close proximity to urethra

(<3mm) as shown in Figure 2.4. It is reasonable to assume that this has pushed the dose gradient to the limit of what can be physically achieved.

The exact value of α/β for prostate cancer is currently being debated. To address this uncertainty, low α/β ratio plans (based on Set II Table 2.2) were also generated using data from three patients using the same EUD prescription and priorities.

Table 2.7 Comparison of EUD (Gy) between high and low prostate α/β ratio plans

	PTV		Bladder		Rectum		Urethra	
	α/β=8.33	α/β=1.5	α/β=8.33	α/β=1.5	α/β=8.33	α/β=1.5	α/β=8.33	α/β=1.5
Patient#4	85.30	86.00	30.45	30.02	53.90	54.05	64.54	63.55
Patient#5	84.17	85.98	25.09	24.30	55.23	56.06	64.94	63.91
Patient#6	86.21	86.94	29.79	28.40	57.91	56.17	63.51	62.83

Data in this table shows that for both high and low α/β ratios, there is no significant difference in final EUD for PTV and biological outcome between two sets of plans.

Several parameters used in the hypoxia model were changed to cover a broad range. EUD of PTV is recalculated for patient #1 after the change of each parameter and listed in the following table.

Table 2.8 PTV_EUD change after change of model parameters

Original Value	Hypoxic portion of PTV_Ah		T		Hypoxic fraction of a complete pO_2 cycle		B	
	70%		10min		60%		10%	
EUD (Gy)	83.77							
Modified EUD (Gy)	50%	90%	5min	20min	40%	80%	2%	30%
	81.89	84.26	83.51	83.70	83.59	84.66	87.27	80.08

Hypoxic portion of PTV_Ah is the portion of true acute hypoxic volume in PTV_Ah as it is assumed that hypoxic voxels are discretely distributed. T is the period of a complete pO_2 cycle and hypoxic fraction gives out the time fraction of hypoxic state in this cycle. *B* is the re-oxygenation ratio of chronic hypoxic cells after each fraction. Data in the table show that changes in most of the parameters (except re-oxygenation ratio)

don't have a significant impact on target EUD. It is clear that a larger value of the parameter B will lead to an oxygenated PTV_Ch volume after 20-30 fractions whereas smaller values will maintain the hypoxic status of the PTV_Ch volume. As these parameters make tumors more resistant, EUD of PTV is also getting higher, which suggests that in this circumstance dose painting is more effective than giving uniform dose in the PTV. For patient #1, two plans were re-optimized based on listed *B* values (Table 2.8). EUD of PTV was maintained in both plans (for B=2% plan EUD=85.62Gy, for B=30% plan EUD=86.41Gy), and this is achieved without EUD increase for rectum and urethra (for both plans, EUD for rectum and urethra were maintained at 59Gy and 63Gy respectively)

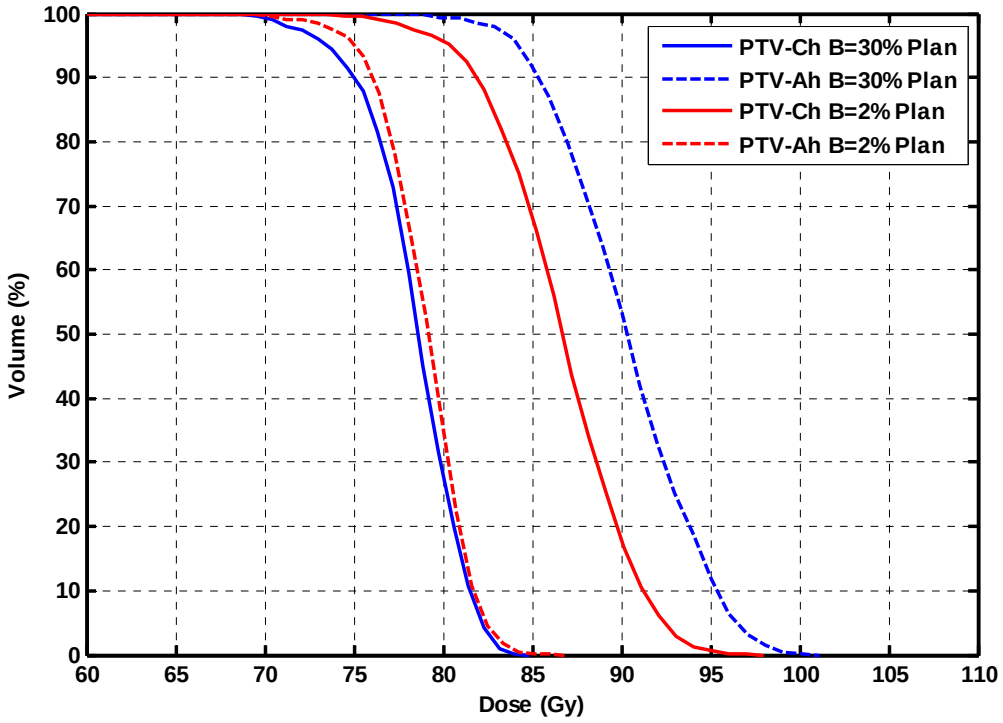

Figure 2.10: DVH comparison of BGRT plans based on two different re-oxygenation ratios of chronic hypoxic cells. Red lines are DVH for PTV_Ah volume. Blue lines are

DVH for PTV_Ch volume.

From Figure 2.10, it is clear that for the *B*=2% plan, dose in the chronic hypoxic volume is maintained at a high level as it is shown in Figure 2.6, the acute hypoxic volume is considered less resistant and receives a smaller dose. For *B*=30% plan, since most chronic hypoxic cells are oxygenated after several fractions, PTV_Ch receives less dose than the previous plan, however PTV_Ah is given a much higher dose as a compensate from the unconstrained optimization mechanism to boost the target dose. The benefit of this is that EUD of the entire PTV still gets higher than 85Gy in two different settings. As it is shown in Table 2.8 and Figure 2.10, variation in re-oxygenation ratio will have a certain impact on final outcome of tumor control and boosting dose given to both hypoxic volumes should be different in each scenario. This implies that in the conventional dose painting study, prescription dose to chronic hypoxic and acute hypoxic volumes should ideally be varied in accordance to re-oxygenation ratios to maintain the current tumor control and tissue sparing features. In the clinical setting this may be logistically difficult because it will require repeat scans for tumor response including hypoxia patterns. Also, conclusive evidence that repeat imaging carries predictive powers for re-oxygenation has to be collected.

2.4.2. Comparing to Clinical VMAT Plans

Any comparison of unconstrained biological vs. dose-based optimization is prone to certain biases. In this study we compared biologically optimized VMAT plans with dose-based optimized VMAT plans using CT sets from 4 patients. For each patient, the dose-

based optimized VMAT plan is designated to give a uniform PTV dose equal to the EUD of the PTV in the biologically optimized plan, thus two plans will have the same tumor control outcome if the same hypoxic volumes are added on the CT set. The objective was to investigate whether uniformly boosting the entire PTV to the same level comparing to PTV_EUD in BGRT plans will provide the same or better normal tissue sparing as provided by dose-painting using biological optimization. EUD comparison for the 4 patients is shown in Table 2.9. Urethra is excluded in the comparison as it is not considered as an OAR in the dose–based VMAT optimization.

Table 2.9 Comparison of EUD (Gy) between VMAT and biologically optimized (BGRT) plans

	patient #1		patient #2		patient #3		patient #7	
	VMAT	BGRT	VMAT	BGRT	VMAT	BGRT	VMAT	BGRT
PTV[a]	83.07	83.77	80.13	82.19	79.83	80.42	83.01	84.43
Rectum	68.80	60.08	65.31	61.15	68.08	59.91	69.36	61.09
Bladder	35.49	31.45	25.02	23.12	50.10	45.88	34.94	31.78

[a] EUD for PTV in VMAT plans was calculated as the uniform dose which gives the same tumor cell surviving fraction assuming all cells in the PTV are oxygenated, e.g., SF2=0.5248

Compared to conventional VMAT plans, using the proposed method, better normal tissue sparing can be achieved (EUD reduction: 5-9Gy for rectum and 2-5Gy for rectum) when dose in PTV is boosted to the same level. Note that as was stated above, urethra is acting as a dose limiting factor in BGRT plans whereas it is not included in VMAT plans. It is reasonable to believe that if urethra was not taken into account, dose in PTV can be boosted to an even higher level, in other words, providing superior normal tissue sparing compared to conventional IMRT plans if the same EUD in PTV was achieved in latter plans.

In this study, we assumed that the hypoxia related parameters remain stable during the course of treatment. Several studies suggest that there is a notable fluctuation of these

parameters in actual treatments. However, as demonstrated above, the proposed dose painting approach is not sensitive to it, therefore further providing the possibility to adapt hypoxic related biological parameters during the entire treatment. The comparison of different re-oxygenation ratio plans suggests that different dose levels in acute hypoxic and chronic hypoxic volume are required to preserve target coverage and critical tissue sparing in the presence of various re-oxygenation ratios. Dose painting in the conventional approach would be a choice, however as demonstrated above, it is difficult to determine the dose level needed in different hypoxic volumes as the optimal dose level varies in different scenarios. Giving a boosting dose to the entire PTV volume would be a simple solution, however as also demonstrated above, it comes with inferior normal tissue sparing in rectum and bladder. Both obstacles are surmounted in the proposed approach.

2.5. Conclusion

A dose painting approach using BGRT was proposed based on the modified hypoxia model. From the comparison of conventionally optimized plans using the same dose delivery technique, we demonstrated that this proposed approach is suitable for dose painting purposes in terms of maintaining superior tumor control and normal tissue sparing. Although in this study, we adopted biological modeling parameters from *in-vivo* measurement and animal models, which is main drawback of this study. The robustness of this approach was proven for a range of parameters describing hypoxic conditions.

The geometric uncertainties associated with patient set-up error and organ motion will result in the dose distribution shift from systematic uncertainties and blurring from random uncertainties. This means that the normal tissue sparing dose closely conformed

to urethra might move into PTV due to the organ motion and patient set-up error. This might have a negative impact on the overall clinical outcome. The purpose of this planning study was to fully explore the dose sparing/boosting which can be achieved if EUD-based biological optimization is applied to drive a solution for VMAT dose delivery. In this study we pushed the requirement for biological conformality to the limit. The target volume was surrounded by two critical structures, contained hypoxic areas inside and yet one more critical structure located inside the target volume. We showed that it was possible to achieve a sharp dose gradient, boost dose in hypoxic cells and spare urethra. Studies to account for geometric uncertainties are reported in Chapter 3.

CHAPTER 3. Geometrical Uncertainty Adapted BGRT Optimization

3.1. Geometrical Uncertainty in Radiation Therapy

In Intensity Modulated Radiation Therapy (IMRT), dose is usually delivered to patients in multiple fractions. The main advantage of IMRT is that it creates dose gradients which can be utilized to conform high dose regions to target volumes while efficiently sparing normal tissue. These high dose gradients may cause over-exposure of organs at risk and underdosing of target volumes in the case of a geographical miss. Thus, exactly reproducing patients' daily position before the treatment is essential to ensure the dose coverage of target volumes in every fraction and the quality of the treatment. However, exact realignment of patients' position is difficult. While small set-up errors, which are of the same magnitude for all patients, are unavoidable and are accounted for in the PTV margin, errors associated with organ motion are patient-specific and require image-guidance for corrective action. Generally, the geometrical errors associated with radiation therapy can be categorized as systematic error and random error.

Systematic error accounts for the difference in patient's position in the full treatment and the CT scan used for RT planning. This error is propagated through all treatment fractions. The planning CT scan is performed before the treatment and is a snapshot of patient's anatomy at a particular moment in time. Tumor volume and normal tissues are delineated on the planning CT. For target volume the systematic error can be interpreted as misalignment between average position of the target volume through the treatment and the position at the time of planning CT. In addition to daily variations in patient's anatomy it also accounts for laser misalignment between CT and treatment room. The

goal of radiation therapy is to deliver a curative dose to the target as indicated in the planning CT scan. If the patient's position is different from the position in the CT scan because of set-up error, the dose delivered will not cover the desired target and causing underdose in the PTV and overdose in normal tissue (Figure 3.1). Shifting the dose matrix based on systematic uncertainty data can adequately simulate this effect.

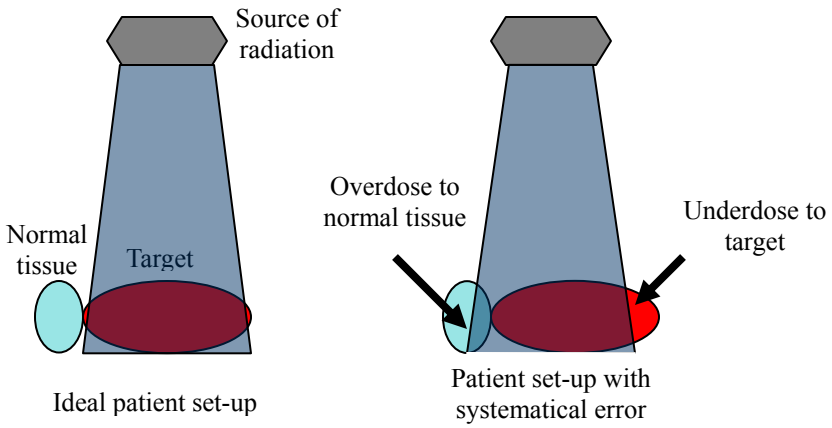

Figure 3.1 Illustration of underdose and overdose caused by systematic error in patient set up.

In clinical practice, in-house laser systems and tattoos drawn on the patient's body are used for a reproducible set-up to skin marks. The residual small error in set-up is assumed to be of a random nature, i.e., if one day laser would be slightly anterior to the tattoo, next day it would be posterior with a net misalignment close to zero. In addition to these random set-up uncertainties internal organ motion including respiration, diaphragm movement and peristaltic movement can cause random error which represents the displacement of the target between fractions and during the treatment. Even if the setup errors to external skin marks are eliminated, random errors from internal organ motion can still result in un-desired reduction of target coverage (Figure 3.2). Assuming

homogeneous tissue and intra-fraction motion only, convolution of the static dose distribution with a probability density function based on random error has been suggested as an efficient approach to estimate the actual dose distribution. The error between dose in direct simulation and corrected convolution can be minimized to 3% [51].

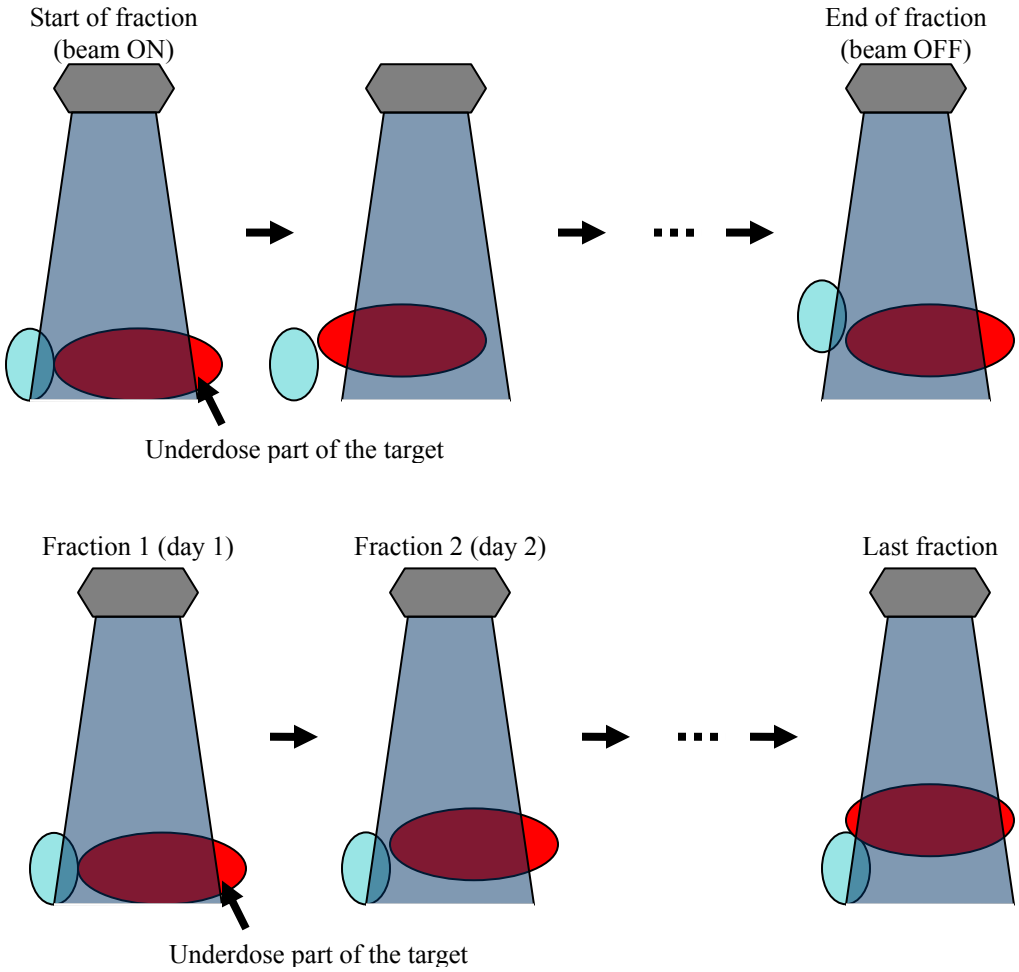

Figure 3.2 Illustration of underdose caused by random errors (Top panel: effect of intra-fraction motion in one single fraction. Bottom panel: effect of inter-fraction motion in the entire treatment course)

3.1.1. Mathematical Background in Systematic and Random Error

If real time images can be obtained during the treatment, patient's position and geometrical errors would be available. Mathematically, systematic error can be calculated as a difference between tumor location defined on the planning CT and mean location after *n* fractions. Random error for each fraction is calculated as a difference between mean location after *n* fractions and location in the considered fraction.

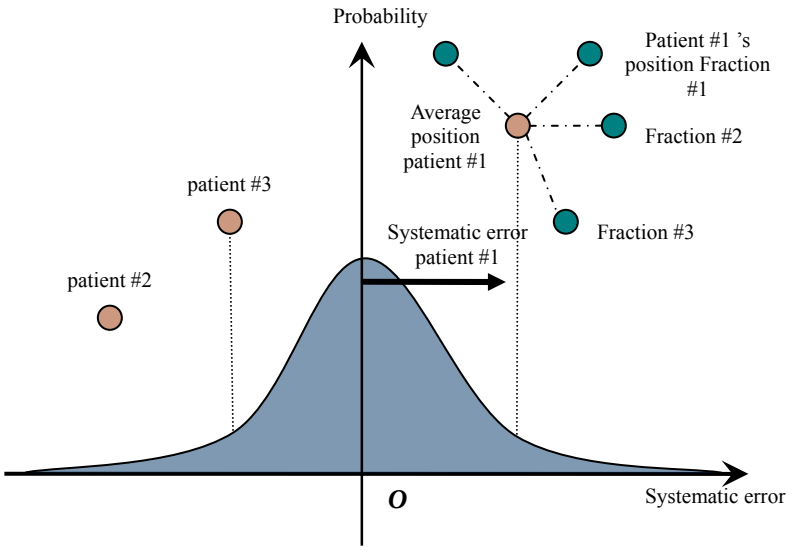

Figure 3.3 Systematic error of a population are assumed to obey a Gaussian distribution. The standard deviation of this distribution is usually reported, whereas its mean value equals zero if an on-line protocol is adopted.

Mean systematic error is expected to converge to its expectancy value after a sufficient number of portal images are taken. Population-based systematic error is expected to be distributed as a Gaussian in each of three dimensions, therefore standard deviation for this distribution can be also derived after a sufficient number of patients is followed-up. Note that, systematic error is expected to approach zero if an on-line

protocol is applied (see Section 3.2).

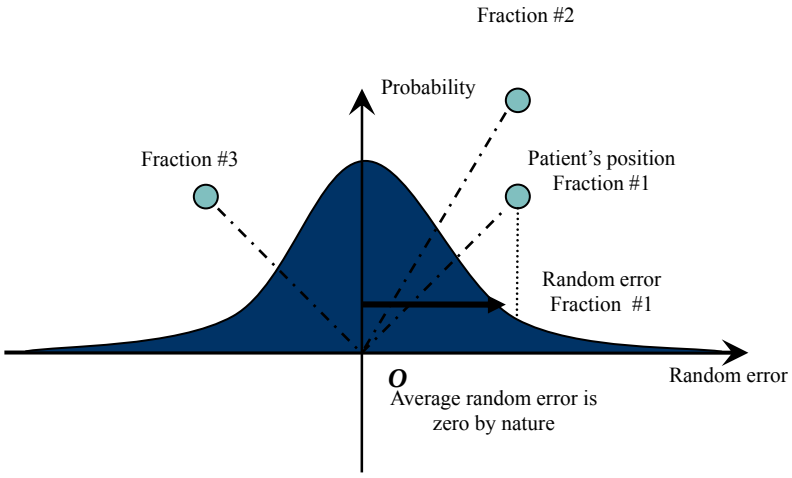

Figure 3.4 Random error also obeys a Gaussian distribution, whereas its mean value is zero by definition.

Expectancy value for random error is zero by definition. Therefore, standard deviation of random error recorded in each fraction is usually reported and used to describe random error (Figure 3.4). This means that each patient followed through the treatment will provide one value of the systematic error and one standard deviation describing random error. Note that for patients who were realigned and a verification set of portal images was taken, systematic and random errors are available for both before and after realignment.

3.2. Electronic Portal Imaging Device (EPID)

Image Guided Radiation Therapy (IGRT) has served as the primary solution regarding geometrical uncertainties in radiation therapy. Various methods and equipment have been proposed as a supplement to reduce the impact of geometrical uncertainties. Electronic portal imaging devices (EPID) is one of them [52]. The EPID used in this work is an a-Si

imager (Varian Medical Systems) mounted on a linear accelerator. The design of the amorphous silicon (a-Si) portal imager is sketched in Figure 3.5. It can be divided into four major components: a) a thin copper plate; b) a scintillating phosphor screen; c) photodiode and Thin Film Transistor (TFT) matrix; d) Read-out Electronics which outputs the final image matrix. Photon beams exiting from the patient will first interact with the metal build-up layer which is usually 1mm thick of copper. The purpose of the copper layer is that Compton electrons can be set in motion by entering photon beams, meanwhile scatter radiation which may contribute to noise in the image is absorbed. The incident radiation is further converted into light signal in the scintillating screen, whereas the pixel matrix which contains one photodiode and one TFT in each pixel transfers light input into electric charges. The charge is read out one row a time and is subsequently converted into a digital signal by read-out electronics (Figure 3.5).

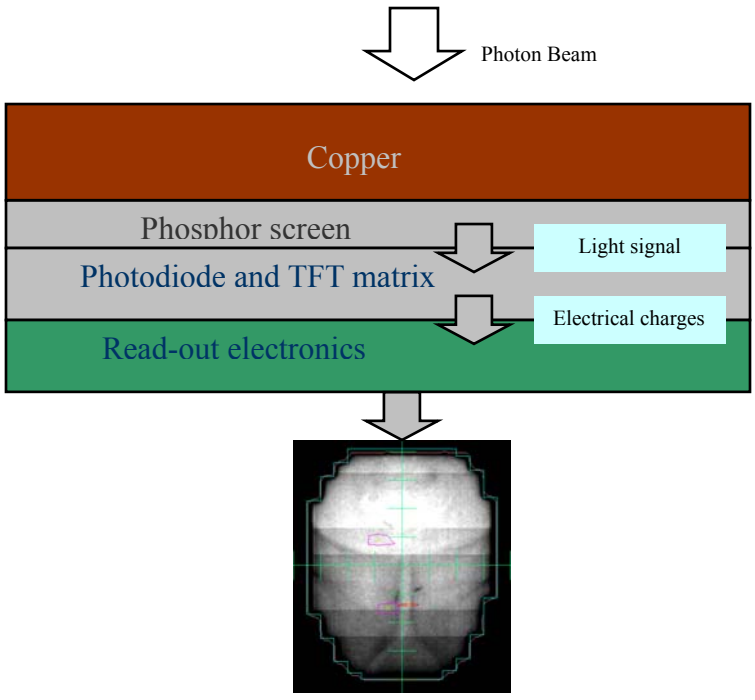

Figure 3.5 Cross sectional view of a-Si detector.

EPID can be used to verify both the position of a patient and dose delivered to the patient during the therapy. When a patient with prostate cancer is treated with radiation therapy, EPIDs can be used with implanted markers to verify prostate position, realign a patient if required, and thereby reduce geometrical uncertainties. Three gold fiducial markers are implanted into the patient's prostate under ultrasound guidance prior to acquisition of the planning CT scan. Typical locations for the markers are right apex, left middle and right base of the gland. At least three days are allowed between implantation and CT scan for edema to subside. After the treatment plan is produced, digitally reconstructed radiographs (DRR) with contoured fiducial markers are generated from the planning CT and are taken as the reference. In the following fractions, daily portal images are collected before delivering the dose. The error of prostate position compared to planned position can be derived by comparing the position of fiducial markers in the reference DRR and newly acquired image. A variety of protocols has been explored with off-line and on-line corrections as a basis for corrective action. In off-line protocols images are acquired for the first few, typically three to five, fractions and moves are derived from the average misalignment. The main purpose of this protocol is to effectively eliminate systematic uncertainties. The underlying assumptions are that 1) the first few fractions are sufficient to establish the "true" location of the prostate; 2) random errors due to set-up uncertainties and organ motion are not as important compared to systematic errors and are accounted for in PTV margins; 3) mean location of prostate does not change in systematic fashion in the process of RT. On-line protocols require taking portal images prior to every fraction. Typically no corrective action is performed if misalignment is less than a pre-set threshold, e.g., 3mm. The benefit of this approach is

that it accounts for systematic and random inter-fraction uncertainties, however, it is more time consuming. An on-line protocol has been implemented at the BCCA, therefore misalignment data are available for every fraction.

3.3. Geometrical Uncertainty Adapted Optimization Method

3.3.1. Materials

This study is based on the CT images and contours from our previous BGRT dose painting study on prostate tumor hypoxia (Chapter 2). CT sets and organ contours from patients in that study were selected. Hypoxic volumes were left unchanged. Urethra contours were extended to the bottom of bladder and PTV by radiation oncologists whereas in our previous study, urethra was only contoured inside the CTV. PTV contours were extended to cover the previous PTV volume plus 0.5cm margin on urethra for the precise reconstruction of the dose both in CTV and urethra after the dose matrix is shifted and convolved. This PTV serves only as a surrogate for a limited region for convolution to reduce computational burden. Because systematic and random errors are simulated during the optimization, curative dose coverage of PTV is no longer the main planning objective. A thin shell-shaped structure "PTV_Shell" created as a 5mm isotropic 3D expansion of PTV was also created to avoid undesired hot spots (>80Gy) outside the PTV. Five plans from the previous study were selected and re-optimized in this study. Results from our previous study were used for comparison purposes.

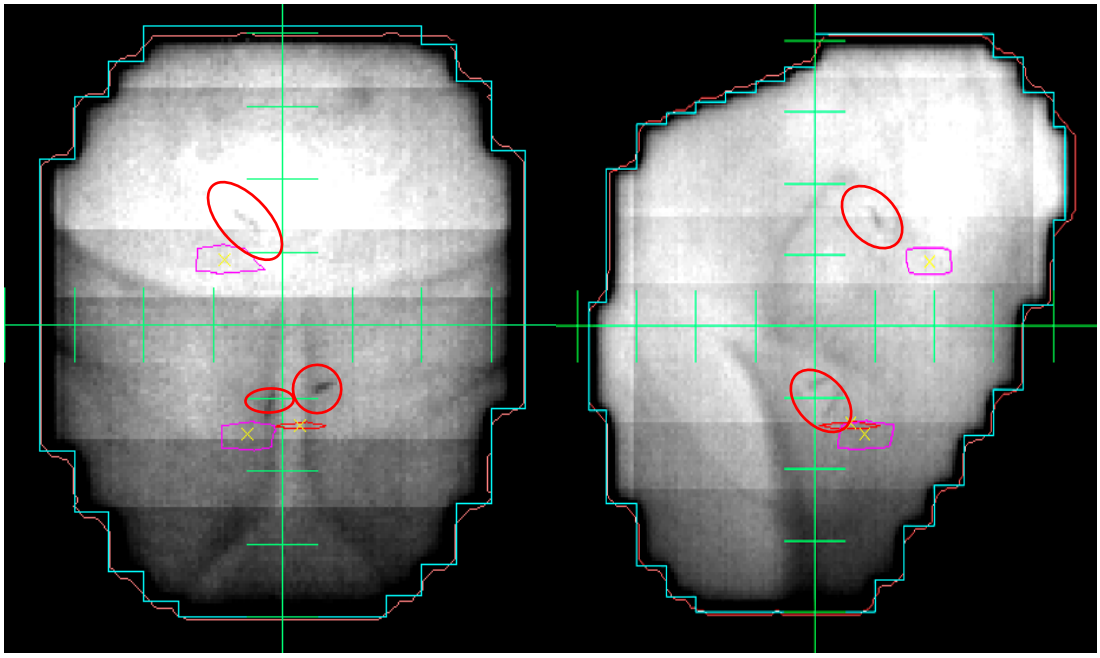

Figure 3.6 The positions of fiducial markers in reference images (contoured in purple) and acquired images before daily treatment (black ribbons with red contours). Right panel shows anterior field, left panel shows lateral field.

Portal images were acquired prior to each fraction, as it is shown in Figure 3.6. The difference between actual positions of fiducial markers (dark ribbons in the image) and positions in DRRs generated from the RT plan (purple colored contour) were used to calculate misalignment in three dimensions. All daily misalignments were recorded. For patients who were realigned repeat portal images were taken to validate that residual misalignment is below an action level (3mm). Residual errors were also recorded. Some patients showed a persistent misalignment indicative of a systematic error. In these cases mean misalignment was calculated and an appropriate shift was applied prior to taking the first set of portal images. This procedure is described as a global shift because it applies to all remaining fractions. All global shifts made during the course were also recorded and added to the image errors exported from treatment planning systems, thus

systematic errors of the entire course can be derived.

3.3.2. Methods

Mean systematic and random error can be calculated using misalignment σ_i acquired at *i*th fraction:

$$\overrightarrow{\sigma_{sys}^{n}} = \frac{1}{n}\sum_{i=1}^{n}\overrightarrow{\sigma_i} \quad , n = 5,10,15,20,...,35 \quad (3.1)$$

$$\overrightarrow{\sigma_{rand}^{n}} = \sqrt{\frac{1}{n}\sum_{i=1}^{n}\left(\overrightarrow{\sigma_i} - \overrightarrow{\sigma_{sys}^{n}}\right)^2} \quad , n = 5,10,15,20,...,35 \quad (3.2)$$

During the optimization, the entire dose matrix in PTV is shifted based on systematic error $\overrightarrow{\sigma_{sys}} = (x_0, y_0, z_0)$ before each iteration.

$$D_{shifted}(x,y,z) = D_{static}(x - x_0, y - y_0, z - z_0) \quad (3.3)$$

This process simulates the set-up error prior to the delivery of dose and this shift remains unchanged during the entire treatment plan optimization.

To simulate random error, the probability of that voxel at position (x,y,z) moves to position (x',y',z') can be calculated using random error $\overrightarrow{\sigma_{rand}} = (\sigma_x, \sigma_y, \sigma_z)$:

$$\mathrm{pdf}(x,y,z,x',y',z') = \frac{1}{2}\left[\mathrm{erf}\left(\frac{x - x' + \frac{\Delta x}{2}}{\sigma_x\sqrt{2}}\right) - \mathrm{erf}\left(\frac{x - x' - \frac{\Delta x}{2}}{\sigma_x\sqrt{2}}\right)\right] \cdot \frac{1}{2}\left[\mathrm{erf}\left(\frac{y - y' + \frac{\Delta y}{2}}{\sigma_y\sqrt{2}}\right) - \mathrm{erf}\left(\frac{y - y' - \frac{\Delta y}{2}}{\sigma_y\sqrt{2}}\right)\right]$$
$$\cdot \frac{1}{2}\left[\mathrm{erf}\left(\frac{z - z' + \frac{\Delta z}{2}}{\sigma_z\sqrt{2}}\right) - \mathrm{erf}\left(\frac{z - z' - \frac{\Delta z}{2}}{\sigma_z\sqrt{2}}\right)\right]$$

(3.4)

where Δx, Δy, Δz are voxel size and σ_x, σ_y, σ_z are standard deviations of geometric uncertainty in each direction (Lat, AP, SI). This probability density function is pre-calculated for each voxel in PTV prior to optimization and is independent of dose distribution. Therefore, dose shifting and blurring during the optimization as it was in the treatment planning software mimics treatment of a particular patient inclusive of geometrical uncertainties and produces a plan accounting for these uncertainties. The realistic dose metric which is substituted into the cost function can be calculated by

$$D_{realistic}(x,y,z) = \sum_{x',y',z'} D_{shifted}(x',y',z')\,\mathrm{pdf}(x',y',z',x,y,z) \quad (3.5)$$

Plan optimization was based on the same procedure introduced in Chapter 2. Total dose is delivered in 35 fractions. The dose per fraction in the *i*th voxel d_i is:

$$d_i = D^i_{realistic} / n \quad (3.6)$$

where n is the number of fractions. Normalized total dose (NTD) is derived based on Eq. 2.5:

$$NTD_i = D^i_{realistic} \frac{\alpha/\beta + d_i}{\alpha/\beta + 2\mathrm{Gy/fr}} \quad (3.7)$$

where D_i is the dose delivered to voxel *i* in 35 fractions. Values of α/β were set to 3Gy for all normal tissues except urethra (which is assumed that *NTD* equals total dose here) since there is insufficient supporting data.

Tumor cell density was assumed to be uniform inside the CTV, therefore overall tumor cell surviving fraction, accounting for effects of hypoxia, can be described as:

$$SF = (1 - AHF - CHF) \times SF^{ox} + AHF \times SF^{ah} + CHF \times SF^{ch} \quad (3.8)$$

AHF, CHF are pre-treatment fractions of acute hypoxia (*ah*-) and chronic hypoxia (*ch*-)

cells in CTV. This is different from Chapter 2, where *AHF* and *CHF* are defined as the hypoxic fraction in PTV.

The objective function for unconstrained biologically-based optimization was formulated as:

$$F = \prod_i f_i \times f_h^{ox} \times f_h^{ah} \times f_h^{ch} \quad (3.9)$$

$$f_i = \begin{cases} \left[1 + \left(\frac{EUD_0}{EUD}\right)^{\gamma}\right]^{-1}, \text{for tumor} \\ \left[1 + \left(\frac{EUD}{EUD_0}\right)^{\gamma}\right]^{-1}, \text{for normal tissue} \end{cases} \quad (3.10)$$

where f_h^{ox}, f_h^{ah} and f_h^{ch} are dose inhomogeneity control factors which were explained in Chapter 2. During early stages of implementation of this study, un-desired hot spots (>80Gy) were found outside previously contoured PTV volumes. To avoid this, an RT structure named PTV_Shell was added on CT images. It is a hollow shell which does not designate any particular organ and is intended for optimization purposes only. We further assumed it to be an organ sensitive to hot spots (n=0.06).

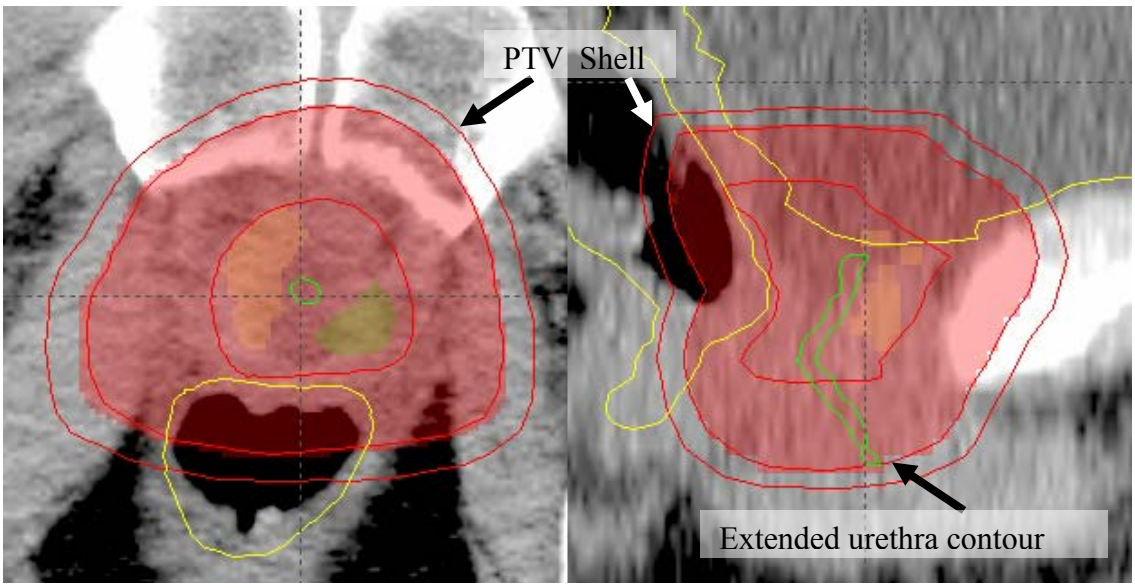

Figure 3.7 Transversal (left) and sagittal (right) view of structure contours in CT images. Hypoxia volumes remain unchanged. The urethra contour is extended to the bottom of the PTV. A new contour PTV_Shell is added.

The parameters used in the optimization are shown in Table 3.1. For a perfect treatment plan, *F* will approach unity.

Table 3.1 Optimization Parameters.

	n (Burman et al)	EUD_0	γ
Bladder	0.5	65	5
Femoral Head	0.25	52	5
Rectum	0.12	45	15
Urethra	0.06	65	15
PTV_Shell	0.06[a]	70	15
CTV	-	80	30

[a] n equal to 0.06 for PTV_Shell are chosen to eliminate hot spots outside CTV.

These dose inhomogeneity control parameters are shown in Table 3.2

Table 3.2 Dose inhomogeneity control parameters used in Eq.2.13

	Tolerable dose inhomogeneity (μ)	Priority (γ)
Oxygenated CTV volume	5%	7
Acute hypoxia volume	10%	5
Chronic hypoxia volume	10%	5

3.3.3. Results

Cumulative systematic errors for five patients calculated from the mean of accumulated image errors with five fraction increments are shown in Figure 3.8 below.

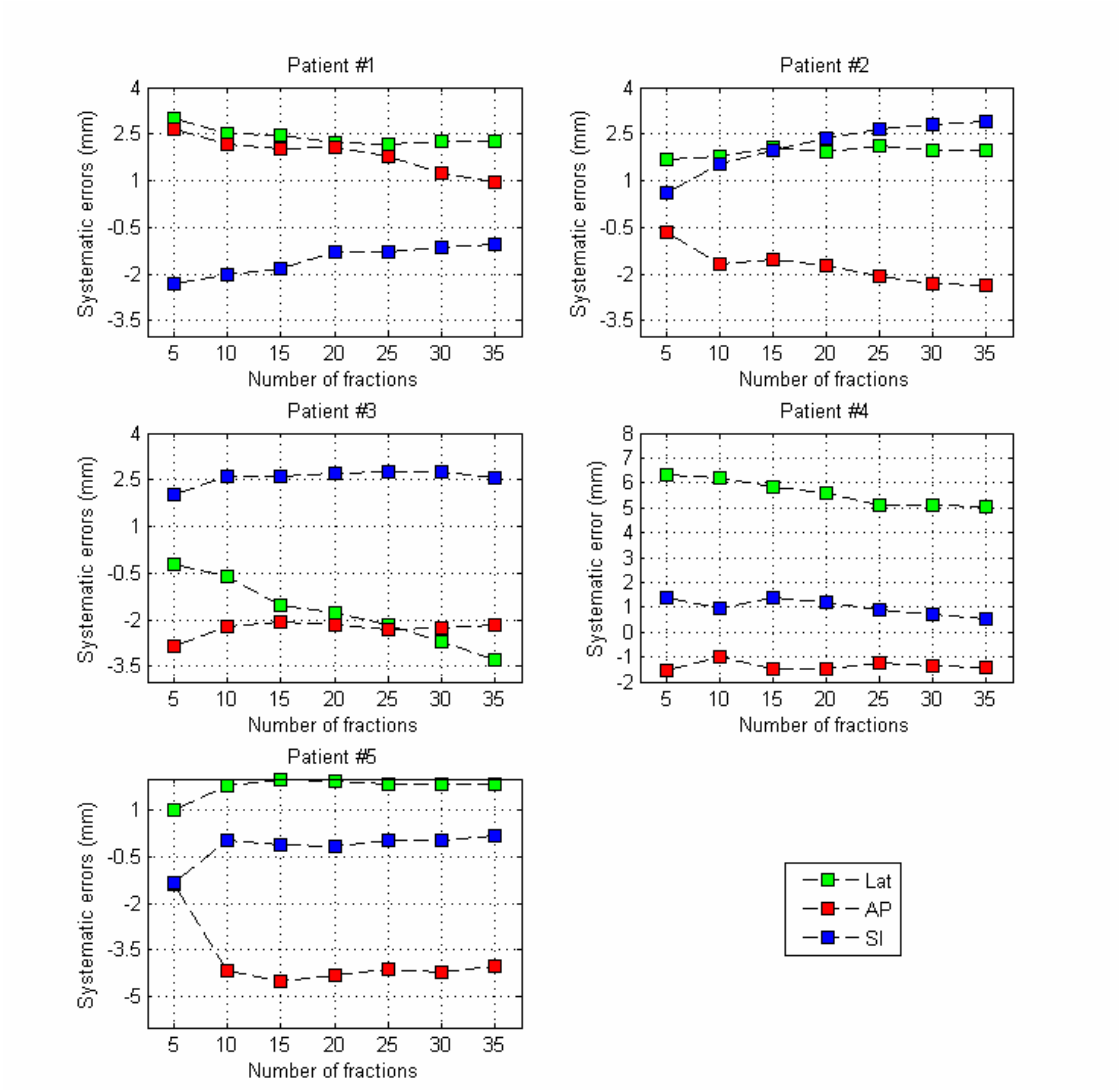

Figure 3.8 Systematic errors as a function of number of fractions

Cumulative random errors after every five fractions can be calculated as standard deviations of cumulated image errors (Figure 3.9):

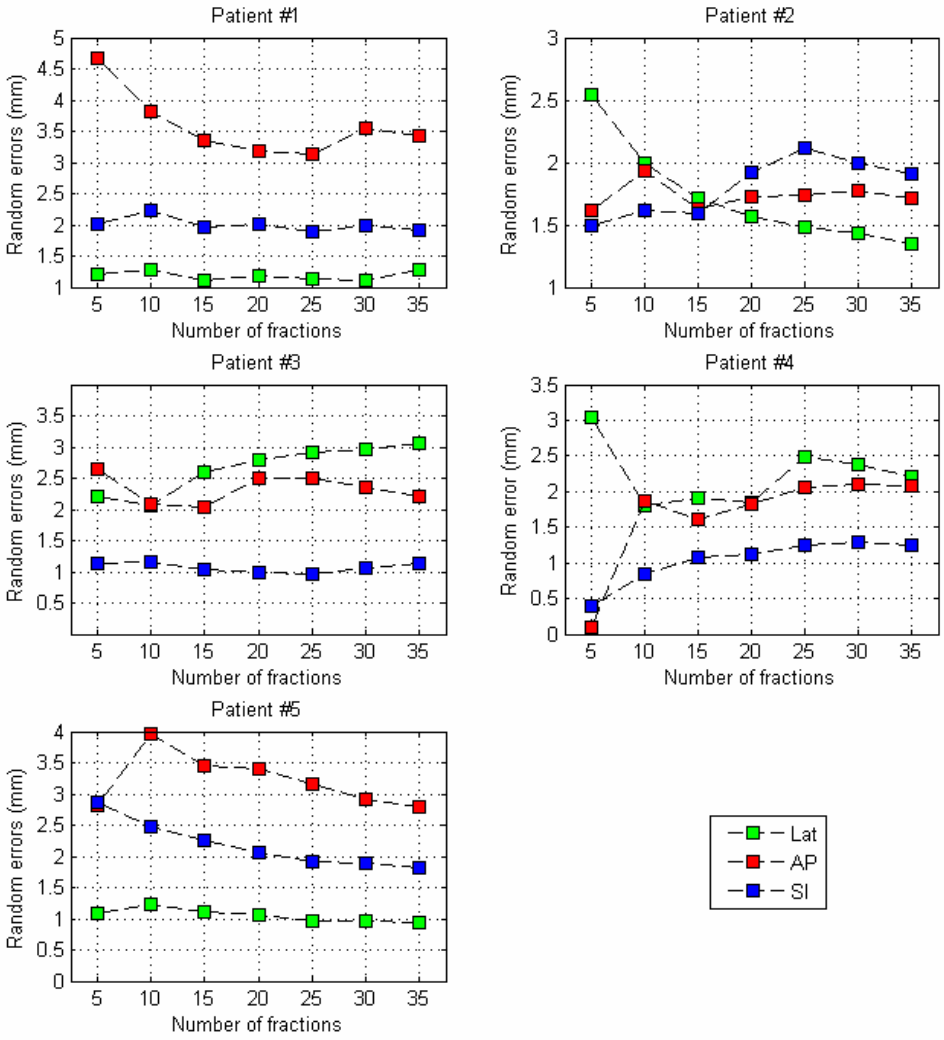

Figure 3.9 Random errors as a function of number of fractions

Using acquired systematic and random errors after 35 fractions, EUD in CTV and urethra as defined in our previous study (see Chapter 2) were recalculated, Table 3.3.

Table 3.3 EUD(Gy) comparison of static plans with/without dose shifting and blurring

	CTV		Urethra	
	Static	Adapted	Static	Adapted
Patient #1	83.00	80.83	70.75	71.57
Patient #2	82.20	80.30	73.23	73.12
Patient #3	81.47	77.19	74.38	78.15

Patient #4	82.33	78.23	67.90	77.69
Patient #5	79.52	76.86	71.86	75.13

Static refers to the EUD from the original plans, whereas adapted EUD refers to the EUD of the same plans after dose matrices were shifted and blurred. Note that in this study, urethra contours were extended and cover the high dose volume which was previously considered as PTV. Thus, the shown static urethra EUD is different from values shown in our previous study.

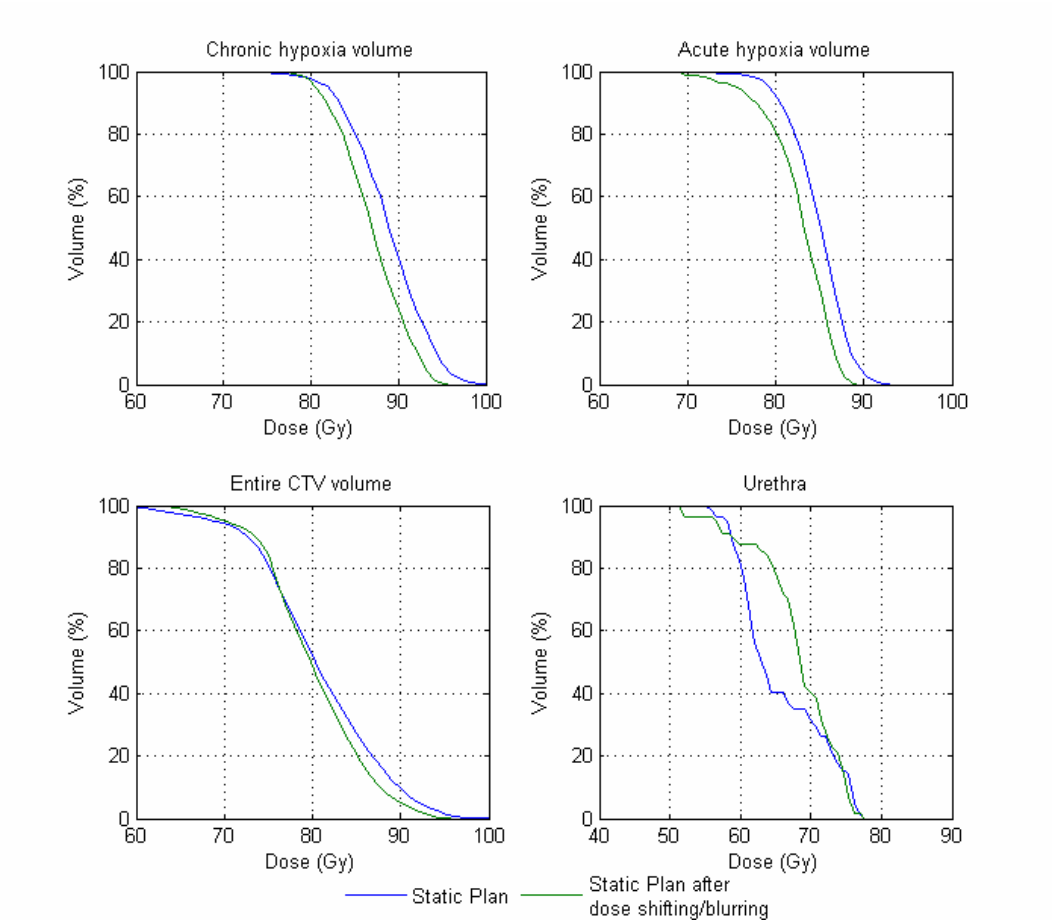

Figure 3.10 DVH comparison of static plans with/without dose shifting and blurring

Since the urethra contour was extended to the PTV in this study it therefore covers a high dose region which shows some hot spots in DVH. From the above DVH comparison

of the same plan with/without set-up and organ motion simulation, we can see that high dose regions corresponding to two hypoxic volumes are smoothed because of convolution with random errors whereas lower dose region corresponding to urethra which is close to the hypoxic volume gets a larger high dose volume than static plans. Using our proposed optimization methods, we were able to simulate systematic and random geometrical errors during the optimization, thus a realistic dose distribution rather than an idealized static dose distribution can be substituted into the cost function. Most important of all, since organ motion and set-up errors are already accounted for in RT planning, PTV margin can be removed from RT planning which leads to a significant dose reduction in rectum. The EUD for CTV, urethra and rectum after dose shifting and blurring are shown in Table 3.4.

Table 3.4 EUD (Gy) comparison of static plans and geometrical uncertainty adaptive plans

	CTV		Urethra		Rectum	
	Static	Adapted	Static	Adapted	Static	Adapted
Patient #1	80.83	79.33	71.57	69.97	61.08	40.57
Patient #2	80.30	79.61	73.12	69.70	61.99	38.52
Patient #3	77.19	78.19	78.15	73.03	61.08	40.78
Patient #4	78.23	77.53	77.69	72.93	62.63	42.74
Patient #5	76.86	76.77	75.13	73.31	59.35	41.80

Static EUD refers to EUD from static plans whereas adapted EUD refers to EUD from plans which accounted for geometrical uncertainties during the optimization, both EUDs were calculated after dose is shifted and blurred. Note that in this study, the convolution volume did not enclose the whole rectum the reported EUD values for this organ are not inclusive of uncertainties, thus rectum dose is calculated as in routine practice which assumes it as a rigid and static organ. In any case the rectum is known as a highly deformable organ, therefore, rigid motion simulation, while reasonable for prostate,

is not realistic for rectum. From the above table one can see that dose coverage is well maintained for CTV between static and adapted plans (EUD difference less than 1.5Gy) whereas dose in urethra is slightly reduced compared to static plans. EUD reduction for rectum is significant (more than 15Gy) because of the elimination of the PTV margin.

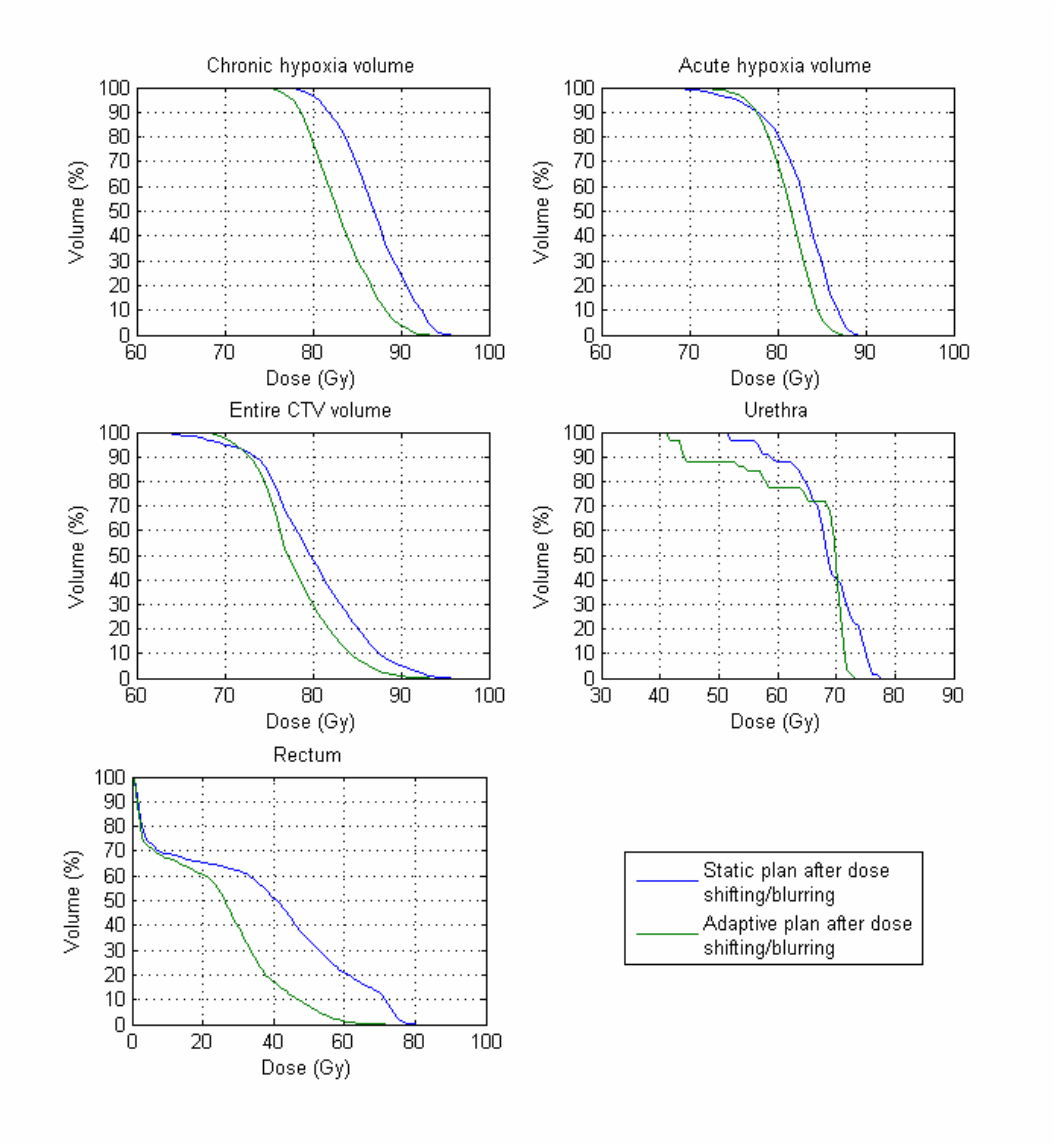

Figure 3.11 DVH comparison of static plans and geometrical uncertainty adapted plans

The proposed method was intended, among other objectives, to eliminate the use of PTV margin to reduce dose in rectum while using a systematic/random error adapted

optimization method to maintain dose coverage in CTV. Systematic/random errors for a particular patient are only available after the entire treatment and image errors of all 35 fractions are collected, however adapting plans to those errors should be carried out before treatment is finished. In our study, for each patient, seven plans were generated using cumulative image errors after every five fractions. Equivalent uniform dose of these plans was recalculated using systematic/random error of the entire 35 fractions. In this way, the outcome of adapting plans during the treatment using incomplete image error data, i.e., from a limited number of fractions, was generated (Figure 3.12).

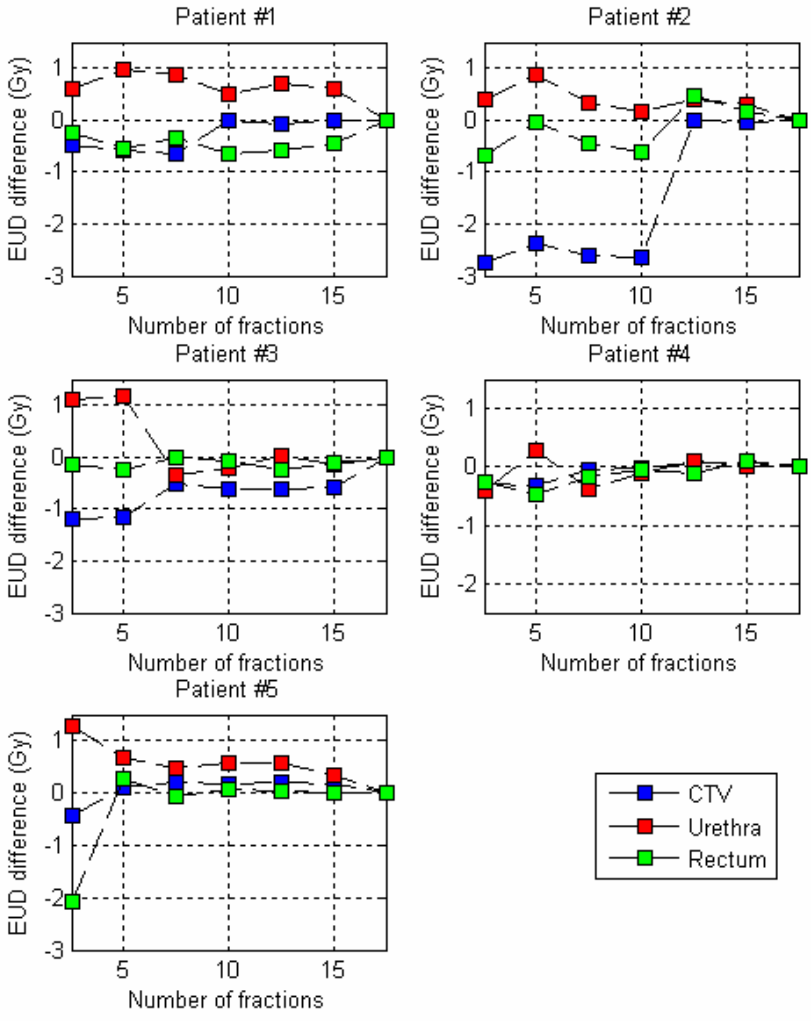

Figure 3.12 EUD history of adaptive plans using geometrical uncertainty collected after a

limited number of fractions with a five fraction increment.

The above figure shows the EUD change for each patient using cumulative image errors acquired during treatment with five fraction increments. The typical differences in EUD of CTV, urethra and rectum are less than 1Gy when limited uncertainty data are adapted in the optimization, except patient #2 where a difference in CTV EUD larger than 2Gy was observed when using uncertainty data from the first 20 fractions.

3.3.4. Discussions

The aim of using PTV margin is to guarantee the curative dose coverage in CTV. The size of this margin in prostate radiation therapy is usually set from population-based systematic and random uncertainties. Several studies have explored the probability distribution of CTV inside PTV. Apparently, giving high dose to all the PTV including some positions where CTV has a small probability to move into is not an efficient approach and might lead to severe normal tissue toxicity. Whereas current on-line correction methods only aim at reducing the geometrical uncertainty, the purpose of this study is to design an optimization method which inherently takes geometrical uncertainty into account on a population or individual basis. We assumed that the prostate is a rigid organ, which is a reasonable assumption. We applied the optimization method to our previous dose painting study in BGRT, however this method can also be applied to other conventional IMRT practices. As was demonstrated above, adapting plans using incomplete, i.e. based on a limited number of fractions, uncertainty data will have outcomes close in terms of tumor control to plans adapted with complete uncertainty data, thus it is feasible to adapt the plans during the initial stages (first five to ten fractions) of

treatment and eliminate PTV margin without compromising tumor control. In our study, we have one OAR inside the CTV and two sub-volumes around this OAR (acute hypoxic and chronic hypoxic regions) which receive dose much higher than CTV. Thus under-dosage in CTV caused by urethra motion can be compensated by hypoxic regions which can also cause over-dose in the CTV due to the motion. We also tried to explore the relationships between EUD of adapted plans and relative change of uncertainties at different fractions, however it appears this problem involves many factors including, systematic error and random error in three directions and relative locations of urethra and hypoxia volumes which are drawn in a random manner.

3.4. Conclusions

A new radiation therapy optimization method was presented in this study. Based on systematic errors and random errors collected with EPID, dose matrices were shifted and convolved with probability density functions during the optimization, thus a realistic dose distribution was substituted into the cost function. Comparison of equivalent uniform dose from treatment plans adapting complete and in-complete geometric uncertainty data was also presented. It was demonstrated that applying this method to produce IMRT-based dose painting plans accounting for partial boosts and normal tissue sparing will at least maintain tumor control while eliminating the use of PTV margin thus achieving a significant dose reduction in rectum.

CONCLUSION

In this thesis, we presented a method based on the concept of biologically guided radiation therapy (BGRT) to overcome prostate tumor hypoxia in intensity modulated radiation therapy (IMRT), see Chapter 2. This method addressed the effect of prostate tumor hypoxia and provided a new approach to combat it. Treatment planning based on the hypoxia model was conducted to evaluate this biologically based RT optimization approach. Although some of the parameters used in this study were adopted from *in vitro* data or other tumor models, the robustness of the proposed method was validated through rigorous sensitivity testing. Evaluation of the treatment plans generated using this method showed that a sufficiently high dose can be delivered to hypoxic tumors in a "dose painting" manner. Meanwhile, urethra and rectum sparing was not compromised with higher dose in the PTV.

In the work presented in Chapter 2, an extremely deep dose gradient was observed as the result of strict constraints on dose escalation to hypoxic volumes and normal tissue sparing. The study regarding the effect of geometrical uncertainty related to this dose gradient was presented in Chapter 3. A new geometrical uncertainty adapted optimization method was also proposed. Although the quality of treatment plans can be compromised by geometrical uncertainty, proposed adaptive optimization methods can inherently take this into account during the optimization thereby reducing the deterioration of plan quality to a minimum. Compared to conventional radiation therapy treatment planning, both methods presented in Chapter 2 and Chapter 3 provide superior outcome as judged by both dose volume indices and equivalent uniform dose.

FUTURE WORK

Numerous theoretical BGRT studies on treatment planning and clinical studies providing biological parameters have been published. The advantage of BGRT is undoubtedly evident and it is seen as the radiation therapy method for the next decade. However, the clinical implementation of BGRT should be taken with tremendous caution. As suggested in a recently published Vision 20/20 paper [53], in the first phase of BGRT clinical trials, target and organs at risk contours should be defined from images with anatomical and functional information. The treatment planning may be conducted using the conventional approach based on dose as an outcome surrogate and requirement of uniform dose coverage in target volumes. Although outcome predictive parameters like EUD, TCP, and NTCP might not be used in treatment planning, they can be used in post-planning evaluation and clinical follow-up [53].

Current commercially available treatment planning programs limit the flexibility and degree of freedom in BGRT research. The development of an in-house treatment planning program for IMRT or conformal radiation therapy is seen as the next step in my research project. This platform should provide the ability to precisely calculate dose distributions and generate high quality treatment plans as compared to commercial treatment planning programs. Its data format should also be compatible with main-stream treatment planning systems and treatment machines. This program will serve as the platform for BGRT research in a broad perspective from image fusion to predictive indices embedded in treatment optimization. As a preparatory stage for this program, SPECT/CT image fusion study and functional burden weighted dose analysis for patients with lung cancer are currently in progress.

REFERENCES

[1]Hall EJ, Giaccia AJ. Radiobiology for the Radiologist. 6th ed. Philadephia USA: Lippincott Williams & Wilkins; 2006.

[2]Nikjoo H, O'Neill P, Terrissol M, Goodhead DT. Modelling of radiation-induced DNA damage: the early physical and chemical event. Int.J.Radiat.Biol. 1994 Nov;66(5):453-457.

[3]Holley WR, Chatterjee A. Clusters of DNA induced by ionizing radiation: formation of short DNA fragments. I. Theoretical modeling. Radiat.Res. 1996 Feb;145(2):188-199.

[4]King CR, Nath R, Rockwell S. Effects of continuous low dose-rate irradiation: computer simulations. Cell Tissue Kinet 1988;21:339-351.

[5]PUCK TT, MARCUS PI. Action of x-rays on mammalian cells. J.Exp.Med. 1956 May 1;103(5):653-666.

[6]Thames HD, Bentzen SM, Turesson I, Overgaard M, Van den Bogaert W. Time-dose factors in radiotherapy: a review of the human data. Radiother.Oncol. 1990 Nov;19(3):219-235.

[7]Nahum AE, Movsas B, Horwitz EM, Stobbe CC, Chapman JD. Incorporating clinical measurements of hypoxia into tumor local control modeling of prostate cancer: implications for the alpha/beta ratio. Int.J.Radiat.Oncol.Biol.Phys. 2003 Oct 1;57(2):391-401.

[8]Orton CG. In regard to Nahum et al. (Int J Radiat Oncol Biol Phys 2003;57:391-401): Incorporating clinical measurements of hypoxia into tumor control modeling of prostate cancer: implications for the alpha/beta ratio. Int.J.Radiat.Oncol.Biol.Phys. 2004 Apr 1;58(5):1637; author reply 1637-9.

[9]Brenner DJ, Hall EJ. Fractionation and protraction for radiotherapy of prostate carcinoma. Int.J.Radiat.Oncol.Biol.Phys. 1999 Mar 15;43(5):1095-1101.

[10]Thames HD, Bentzen SM, Turesson I, Overgaard M, van den Bogaert W. Fractionation parameters for human tissues and tumors. Int.J.Radiat.Biol. 1989 Nov;56(5):701-710.

[11]Michalski J, Purdy J, Bruner DW, Amin M. A phase III randomized study of high dose 3D-CRT/IMRT versus standard dose 3D-CRT/IMRT in patients treated for localized prostate cancer. Radiation Therapy Oncology Group 0126 .

[12]Mohan R, Mageras GS, Baldwin B, Brewster LJ, Kutcher GJ, Leibel S, et al. Clinically relevant optimization of 3-D conformal treatments. Med.Phys. 1992 Jul-Aug;19(4):933-944.

[13]Burman C, Kutcher GJ, Emami B, Goitein M. Fitting of normal tissue tolerance data to an analytic function. Int.J.Radiat.Oncol.Biol.Phys. 1991 May 15;21(1):123-135.

[14]Qiuwen Wu, Lei Xing, Gary Ezzell, Radhe Mohan. Chapter 4 Inverse Treatment Planning. In: Jacob Van Dyk, editor. The Modern Technology of Radiation Oncology: A Compendium for Medical Physicists and Radiation Oncologists. 1st ed. Madison WI: Medical Physics Publishing; 2005.

[15]Marks LB, Sherouse GW, Munley MT, Bentel GC, Spencer DP. Incorporation of functional status into dose-volume analysis. Med.Phys. 1999 Feb;26(2):196-199.

[16]Seppenwoolde Y, Muller SH, Theuws JC, Baas P, Belderbos JS, Boersma LJ, et al. Radiation dose-effect relations and local recovery in perfusion for patients with non-small-cell lung cancer. Int.J.Radiat.Oncol.Biol.Phys. 2000 Jun 1;47(3):681-690.

[17]Woel RT, Munley MT, Hollis D, Fan M, Bentel G, Anscher MS, et al. The time course of radiation therapy-induced reductions in regional perfusion: a prospective study with >5 years of follow-up. Int.J.Radiat.Oncol.Biol.Phys. 2002 Jan 1;52(1):58-67.

[18]Vitali Moiseenko, Joseph O.Deasy, Jacob Van Dyk. Chapter 5 Radiobiological Modeling for Treatment Planning. In: Jacob Van Dyk, editor. The Modern Technology of Radiation Oncology: A Compendium for Medical Physicists and Radiation Oncologists. 1st ed. Madison WI: Medical Physics Publishing; 2005.

[19]Niemierko A. Reporting and analyzing dose distributions: a concept of equivalent uniform dose. Med.Phys. 1997 Jan;24(1):103-110.

[20]Wu Q, Mohan R, Niemierko A, Schmidt-Ullrich R. Optimization of intensity-modulated radiotherapy plans based on the equivalent uniform dose. Int.J.Radiat.Oncol.Biol.Phys. 2002 Jan 1;52(1):224-235.

[21]Lyman JT. Complication probability as assessed from dose-volume histograms. Radiat.Res.Suppl. 1985;8:S13-9.

[22]Kutcher GJ, Burman C. Calculation of complication probability factors for non-uniform normal tissue irradiation: the effective volume method. Int.J.Radiat.Oncol.Biol.Phys. 1989 Jun;16(6):1623-1630.

[23]Schultheiss TE, Orton CG, Peck RA. Models in radiotherapy: volume effects. Med.Phys. 1983 Jul-Aug;10(4):410-415.

[24]Brahme A. Individualizing cancer treatment: biological optimization models in treatment planning and delivery. Int.J.Radiat.Oncol.Biol.Phys. 2001 Feb 1;49(2):327-337.

[25]Kim Y, Tome WA. Risk-adaptive optimization: selective boosting of high-risk tumor subvolumes. Int.J.Radiat.Oncol.Biol.Phys. 2006 Dec 1;66(5):1528-1542.

[26]Otto K. Volumetric modulated arc therapy: IMRT in a single gantry arc. Med.Phys. 2008;35(1):310.

[27]Hall EJ, Wuu CS. Radiation-induced second cancers: the impact of 3D-CRT and IMRT. Int.J.Radiat.Oncol.Biol.Phys. 2003 May 1;56(1):83-88.

[28]Movsas B, Chapman JD, Greenberg RE, Hanlon AL, Horwitz EM, Pinover WH, et al. Increasing levels of hypoxia in prostate carcinoma correlate significantly with increasing clinical stage and patient age: an Eppendorf pO(2) study. Cancer 2000 Nov 1;89(9):2018-2024.

[29]Movsas B, Chapman JD, Hanlon AL, Horwitz EM, Pinover WH, Greenberg RE, et al. Hypoxia in human prostate carcinoma: an Eppendorf PO2 study. Am.J.Clin.Oncol. 2001 Oct;24(5):458-461.

[30]Movsas B, Chapman JD, Horwitz EM, Pinover WH, Greenberg RE, Hanlon AL, et al. Hypoxic regions exist in human prostate carcinoma. Urology 1999 Jan;53(1):11-18.

[31]Dewhirst MW, Braun RD, Lanzen JL. Temporal changes in PO2 of R3230AC tumors in Fischer-344 rats. Int.J.Radiat.Oncol.Biol.Phys. 1998 Nov 1;42(4):723-726.

[32]Brizel DM, Dodge RK, Clough RW, Dewhirst MW. Oxygenation of head and neck cancer: changes during radiotherapy and impact on treatment outcome. Radiother.Oncol. 1999 Nov;53(2):113-117.

[33]Brizel DM, Sibley GS, Prosnitz LR, Scher RL, Dewhirst MW. Tumor hypoxia adversely affects the prognosis of carcinoma of the head and neck. Int.J.Radiat.Oncol.Biol.Phys. 1997 May 1;38(2):285-289.

[34]Wang JZ, Li XA, Mayr NA. Dose escalation to combat hypoxia in prostate cancer: a radiobiological study on clinical data. Br.J.Radiol. 2006 Nov;79(947):905-911.

[35]Yang Y, Xing L. Towards biologically conformal radiation therapy (BCRT): selective IMRT dose escalation under the guidance of spatial biology distribution. Med.Phys. 2005 Jun;32(6):1473-1484.

[36]Tanderup K, Olsen DR, Grau C. Dose painting: art or science? Radiother.Oncol. 2006 Jun;79(3):245-248.

[37]Thorwarth D, Eschmann SM, Paulsen F, Alber M. Hypoxia dose painting by numbers: a planning study. Int.J.Radiat.Oncol.Biol.Phys. 2007 May 1;68(1):291-300.

[38]Ling CC, Humm J, Larson S, Amols H, Fuks Z, Leibel S, et al. Towards multidimensional radiotherapy (MD-CRT): biological imaging and biological conformality. Int.J.Radiat.Oncol.Biol.Phys. 2000 Jun 1;47(3):551-560.

[39]Bucci J, Spadinger I, Hilts M, Sidhu S, Smith C, Keyes M, et al. Urethral and periurethral dosimetry in prostate brachytherapy: is there a convenient surrogate? Int.J.Radiat.Oncol.Biol.Phys. 2002 Nov 15;54(4):1235-1242.

[40]McLaughlin PW, Troyer S, Berri S, Narayana V, Meirowitz A, Roberson PL, et al. Functional anatomy of the prostate: implications for treatment planning. Int.J.Radiat.Oncol.Biol.Phys. 2005 Oct 1;63(2):479-491.

[41]Lee WR, Schultheiss TE, Hanlon AL, Hanks GE. Urinary incontinence following external-beam radiotherapy for clinically localized prostate cancer. Urology 1996 Jul;48(1):95-99.

[42]Fransson P, Bergstrom P, Lofroth PO, Widmark A. Prospective evaluation of urinary and intestinal side effects after BeamCath stereotactic dose-escalated radiotherapy of prostate cancer. Radiother.Oncol. 2002 Jun;63(3):239-248.

[43]Liu M, Pickles T, Berthelet E, Agranovich A, Kwan W, Tyldesley S, et al. Urinary incontinence in prostate cancer patients treated with external beam radiotherapy. Radiother.Oncol. 2005 Feb;74(2):197-201.

[44]Secomb TW, Hsu R, Park EY, Dewhirst MW. Green's function methods for analysis of oxygen delivery to tissue by microvascular networks. Ann.Biomed.Eng. 2004 Nov;32(11):1519-1529.

[45]Yuan H, Schroeder T, Bowsher JE, Hedlund LW, Wong T, Dewhirst MW. Intertumoral differences in hypoxia selectivity of the PET imaging agent 64Cu(II)-diacetyl-bis(N4-methylthiosemicarbazone). J.Nucl.Med. 2006 Jun;47(6):989-998.

[46]Braun RD, Lanzen JL, Dewhirst MW. Fourier analysis of fluctuations of oxygen tension and blood flow in R3230Ac tumors and muscle in rats. Am.J.Physiol. 1999 Aug;277(2 Pt 2):H551-68.

[47]Carlson DJ, Stewart RD, Li XA, Jennings K, Wang JZ, Guerrero M. Comparison of in vitro and in vivo alpha/beta ratios for prostate cancer. Phys.Med.Biol. 2004 Oct 7;49(19):4477-4491.

[48]King CR, Fowler JF. A simple analytic derivation suggests that prostate cancer alpha/beta ratio is low. Int.J.Radiat.Oncol.Biol.Phys. 2001 Sep 1;51(1):213-214.

[49]Ruggieri R, Nahum AE. The impact of hypofractionation on simultaneous dose-boosting to hypoxic tumor subvolumes. Med.Phys. 2006 Nov;33(11):4044-4055.

[50]Emami B, Lyman J, Brown A, Coia L, Goitein M, Munzenrider JE, et al. Tolerance of normal tissue to therapeutic irradiation. Int.J.Radiat.Oncol.Biol.Phys. 1991 May 15;21(1):109-122.

[51]Craig T, Battista J, Van Dyk J. Limitations of a convolution method for modeling geometric uncertainties in radiation therapy. I. The effect of shift invariance. Med.Phys. 2003 Aug;30(8):2001-2011.

[52]Cephas Mubata. Chapter 14 Portal Imaging Devices. In: Philip Mayles, Alan Nahum, Jean-Claude Rosenwald, editors. Handbook of Radiotherapy Physics: Theory and PracticeNew York: Taylor & Francis; 2007.

[53]Stewart RD, Li XA. BGRT: biologically guided radiation therapy-the future is fast approaching! Med.Phys. 2007 Oct;34(10):3739-3751.